Babeș-Bolyai University Cluj-Napoca
Faculty of Physics
Specialization Solid State Physics

DISSERTATION THESIS

Supervisor:
Prof. dr. Lucian Baia

Author:
Codruț-Răzvan Costinaș

2023

Babeș-Bolyai University Cluj-Napoca
Faculty of Physics
Specialization Solid State Physics

DISSERTATION THESIS

Surface characteristics of graphene oxide: a potential protective coating for cultural heritage

Supervisor:
Prof. dr. Lucian Baia

Author:
Codruț-Răzvan Costinaș

2023

ABSTRACT

In recent years, graphene oxide (GO) has emerged as a promising material with diverse applications across various industries. Among its potential uses, one area that has yet to be fully explored is its application as a protective coating for stone cultural heritage. The unique properties of GO, such as its possibility of forming self-assembled films, its barrier effect and chemical stability, make it an ideal candidate for safeguarding stone cultural heritage against degradation. However, before GO can be effectively utilized for this purpose, it is crucial to study its dispersability characteristics. Understanding how GO disperses in different solvents and interacts with stone surfaces is essential for developing efficient coatings that can ensure long-lasting protection without altering the aesthetic and surface integrity of the stone.

Through the use of DLS and ζ-potential measurements, UV-VIS, ATR FT-IR, Raman spectroscopy, XRD, and SEM imaging, the dispersion behavior and the physio-chemical and surface characteristics of as-produced GO and a further refined GO fraction with great self-assembly characteristics was done. Tests were carried out on six dispersions of each GO fraction in water and ethanol mixtures with different vol.% of ethanol (ranging from 0% to 100%).

The performance of GO as a protective coating for stone materials was assessed in accordance with European standards for stone cultural heritage, through which parameters such as water capillary absorption, water vapor permeability, water contact angle, and color variance were investigated for natural and artificially aged samples before and after coating. UV exposure of the coatings was performed to simulate the weathering of the GO coating. Physio-chemical analysis of stone samples and the GO coatings was performed through the use of MIP, FT-IR, Raman spectroscopy, XRD, SEM and optical imaging.

Chapter 1 describes the stone cultural heritage field with its particularities and challenges in finding new coating materials with better protection capabilities as before. An introduction on the characteristics of GO relevant for this field is also made. Chapter 2 first describes the methodology on which the project is based on, and discusses the different stone samples used, as well as the GP syntheses and characterization methods employed. Chapter 3 details and discusses the results obtained in the assessment of GO dispersability and its performance as a protective coating for stone materials. Chapter 4 then provides the conclusions and further perspectives of the study. Overall, GO has shown very promising results as a protective coating for the two types of stones considered, with better results obtained for less porous stone samples.

Contents

Chapter 1

Introduction

1.1 Stone cultural heritage

Cultural heritage refers to the collective wealth of beliefs, traditions, knowledge, customs, artifacts, and practices that are inherited, preserved, and passed down from one generation to another within a particular community, society, or civilization. It encompasses the tangible and intangible expressions of human creativity, encompassing historical sites, monuments, buildings, and other forms of cultural expression that hold significant value and meaning to a group of people. It serves as a reflection of a community's identity, history, and values, fostering a sense of belonging and continuity, while providing insights into the past. Stone cultural heritage comprises a large portion of the tangible cultural heritage, and is represented by a large variation of constructed historical monuments such as buildings and statuary complexes inherited from past generations. The greatest challenges in preserving pristine stone cultural heritage monuments are, generally, the reconstruction or rehabilitation according to original descriptions and the protection against natural causes or the action of pollutants. In this thesis, we will focus on the latter.

Stone, the building block of most historical buildings, might be seen as a stable, indestructible construction material, but it is still subject to natural or anthropological deterioration processes as a result of the simultaneous action of physical, mechanical, chemical or biological agents. Deterioration of stone cultural heritage can be defined as the result of the action of the above-mentioned factors, affecting both the visual aspect of the stone and other "unseen" characteristics such as porosity, mechanical strength or vapor permeability. Ultimately, it is an undesirable process which can lead, in extreme cases, to the complete destruction of the stone material and the structure it comprises.

The mechanisms of deterioration are usually mediated by the presence of water, either through rain or ambient moisture, and have been studied in depth for different types of lithographic materials used in the construction of cultural heritage monuments in literature [1]. The main mechanisms of degradation can be summarized as the following:

- *Mechanical processes:* Usually causing stresses above the mechanical strength of the stone. Includes earthquakes and poor building design, as well as hygric and hydric

swelling, thermal cycling and crystal growth, usually in a combined effect.

- *Chemical processes:* Refer to the dissolution or alteration of the mineral constituents of the stone, due to chemical reactions.
- *Salt action:* Probably the most damaging factor of stone deterioration. Salt formation leads to several of the most destruction forms of stone decay, such as blistering, delamination, scaling, and disintegration.
- *Biodegradation:* Surface damage caused by the presence of a biofilm composed of bacteria, lichens, and fungi, that can have varying effects, from discoloration to dissolution of the stone matrix.

From a historical point of view, deterioration of stone cultural heritage progressed in a natural combination of this factors specific to the local environment until the twentieth century. However, by the mid-twentieth century, the rate of deterioration was accelerated due to the increasing concentration of atmospheric pollutants, such as carbon and sulfur dioxide, or nitrogen oxide and particulate matter, especially in the urban environments [2, 3]. All these serve as catalysts in the occurrence of different chemical reactions at the stone surface, facilitated by the presence of water. Ultimately, water can be considered the most important deteriorating agent, as it triggers most deterioration mechanics, from freeze-thaw cycles to salt crystallization or other chemical reactions inside the stone, as it readily allows diffusion of contaminants inside the stone microstructure [1]. There is also clear consensus that climate change is negatively affecting the built cultural heritage, as a result of the changes in rainfall regime, risk of flooding and other extreme weather effects [4, 5], posing additional challenges in maintaining pristine stone built monuments.

The conservation of stone cultural heritage involves different strategies, depending on the characteristics of the monument, ranging from reconstruction of ruined structures to applying various treatments, either with the goal to restore or improve the mechanical strength of deteriorated stone, or to protect it against chemical mechanisms of deterioration. Broadly viewed, several steps of conservation can be identified, depending on the specifics of the monument [6]. The first step consists of the assessment of the current state of the historical surfaces or structures, which has the goal of identifying the critical risks of degradation and the petrographic composition of the monument. Then, after a thorough cleaning of the surface, a consolidation treatment is applied, with the goal of restoring the mechanical strength of the stones. As a final step, a protective coating can be applied, thus minimizing the permeation of pollutants or salts inside the stone or even minimizing the biodegradation effect as a result of their antimicrobial properties. Though we have only offered a broad picture on the steps taken in the protection of stone cultural heritage, it is worth mentioning that the petrographic composition imposes a large restriction on the types of consolidants and coatings used. Ultimately, the results depend greatly on the types of stones used, for which only a handful of solutions might be available. Often, a good solution is harder to find for less porous types of stones than stones

with higher porosity. In this context, we will continue the discussion with the role of protective coatings, including some examples of the most used types and challenges in developing new protective treatments.

Protective coatings are comprised of various types of materials applied on the surface of a stone material, with the goal of preventing degradation processes that occur mainly at the interface with the environment [7]. In many cases, the treatment is chosen for a specific purpose dictated by the largest risks of damaging the stone substrate, and can be: water repellent, anti-graffiti, salt inhibitors, anti-fouling, etc. Besides posing no risk for the environment or the workers' health during the application procedure, the protective coatings have to fulfill specific requirements for cultural heritage applications, which have been summarized in the following [7]:

- *Protective efficacy:* The coatings should offer a good degree of efficacy against decay agents such as water, pollutants, soiling and biological contamination. Hydrophobic properties are one of the most sought after parameters when discussing possible coating options for a specific application.

- *Adhesion to the substrate:* The treatment should be able to be homogeneously distributed on the surface of the stone while also penetrating the pores. This becomes a challenge in the case of compact, low porosity stones such as granites or marbles, for which there is a greater risk of agglomeration.

- *No reduction of the water vapour permeability:* Although it is necessary for the coating to penetrate the pores, it should not completely occlude them, thus changing the water vapour permeability characteristic of the stone. It is an absolute necessity to allow the breathability of the stone in order to prevent the water condensation inside the pores. Hygroscopic salts, for example, can crystallize underneath the treated area, causing detachment and loss of adhesion of the treated layer.

- *No modification of the aesthetic properties:* One of the most challenging factors to control is maintaining the optical properties of the substrate, for which no change (colour or gloss) should be observed. In cultural heritage applications, treatments should not produce any noticeable changes for the naked eye.

- *Good durability:* In most cases, the stone substrate is exposed to the environment, which imposes a good durability of the treatment against solar radiation, thermal cycles, and water exposure. A good durability of the coating against environmental factors means lower maintenance costs due to the need to retreat the surface.

- *Retreatability:* Current requirements stipulate that the substrate should not be physically, chemically, or mechanically damaged by the application of the treatment, and the coating itself should not prevent the possibility of applying a different product in the future.

The right protective treatment for a specific application has to fulfill in the best way possible the requirements mentioned above, while taking into consideration the costs and limits on the application methods. While hydrophobic coatings might seem to be the most advantageous category, as they prevent the access of water inside the substrate, thus limiting the action of most deterioration mechanisms, they have been used on a large scale in the past with unsuccessful results [8, 9], mainly in the presence of soluble salts, but also by preventing repair or the application of other treatments. In many cases, hydrophobic surfaces showcase dark vestiges along the channels of running water washing away dust, leading to preferential agglomeration of particulate dust. The consensus today, however, is that protective treatments should be applied in localized areas, such as protruding features, not for entire surfaces [3].

There is a broad spectrum of choice in the case of protective treatments, with or without a consolidation effect. Various types of waxes and oils, acrylates, polyester and alkyd resins, epoxy resins, silicate esters and alkyl-triethoxysilanes have been used with different degrees of durability and protective efficacy [6, 9].

Recently, there has been increasing interest in the use of nanomaterials as protective coatings, usually as additives in a polymer matrix or in combination with other inorganic compounds. Some well-researched examples are TiO_2, Ag, ZnO or MgO nanoparticles, with the goal to obtain super-hydrophobic surfaces [10, 11, 12]. Nanolimes, ($Ca(OH)_2$ nanoparticles), have also shown better consolidating results compared to the standard form of lime, due to the better penetration inside the porous structure of the stone [13]. For surface treatments, research has mainly focused on TiO_2 due to its well-known photocatalytic activity under the exposure of UV light, yielding good pollutant degradation and biofilm repellent properties [14], although many nanostructured systems have shown good antimicrobial results [15].

Nanomaterials can be easily tuned and are an excellent choice for increasing the effectiveness of protective coatings. However, when compared to correctly applied traditional treatments, their high cost and quantity required may not outweigh the benefits, as was concluded recently in the case of nano-TiO_2 coatings [16]. Thus, it's worth mentioning that there are a number of questions to be raised, particularly in terms of cost effectiveness and effects on the environment and human health [17]. Firstly, compared to traditional methods, the manufacture and processing of nanomaterials often require sophisticated and expensive industrial procedures, which would raise production costs. Widespread adoption may be hindered by this additional cost, particularly for large-scale applications. Additionally, the effects of nanoparticles on the environment and health are still to be clarified. The synthesis and application process or subsequent washing could leak nanoparticles into the environment, potentially harming ecosystems and endangering workers' health. There is still little understanding on the long-term exposure effects. Thus, while nanomaterials offer promising advancements in stone protection, their drawbacks in terms of cost efficiency and potential environmental and health risks must be

carefully considered before widespread implementation.

1.2 Graphene oxide as a protective coating

Graphene oxide (GO) is a two-dimensional nanomaterial with potential applications as a protective coating in stone cultural heritage, due to its unique structure and surface characteristics. It has similarities to its graphene parent, as being composed of hexagonal carbon planes, but with a varying degree of structural defects and oxygen functionalities attached (Figure 1.1). The oxygen atoms are covalently bound to the planar carbon atoms, converting them from the sp^2-hybridized state of the graphene planes into the sp^3-hybridized state. For an ideal graphene plane, these oxygen functionalities can be considered defects, but they offer GO many unique characteristics of high interest for practical applications, a great example being its ability to generate stable colloidal solutions due to its hydrophilic character.

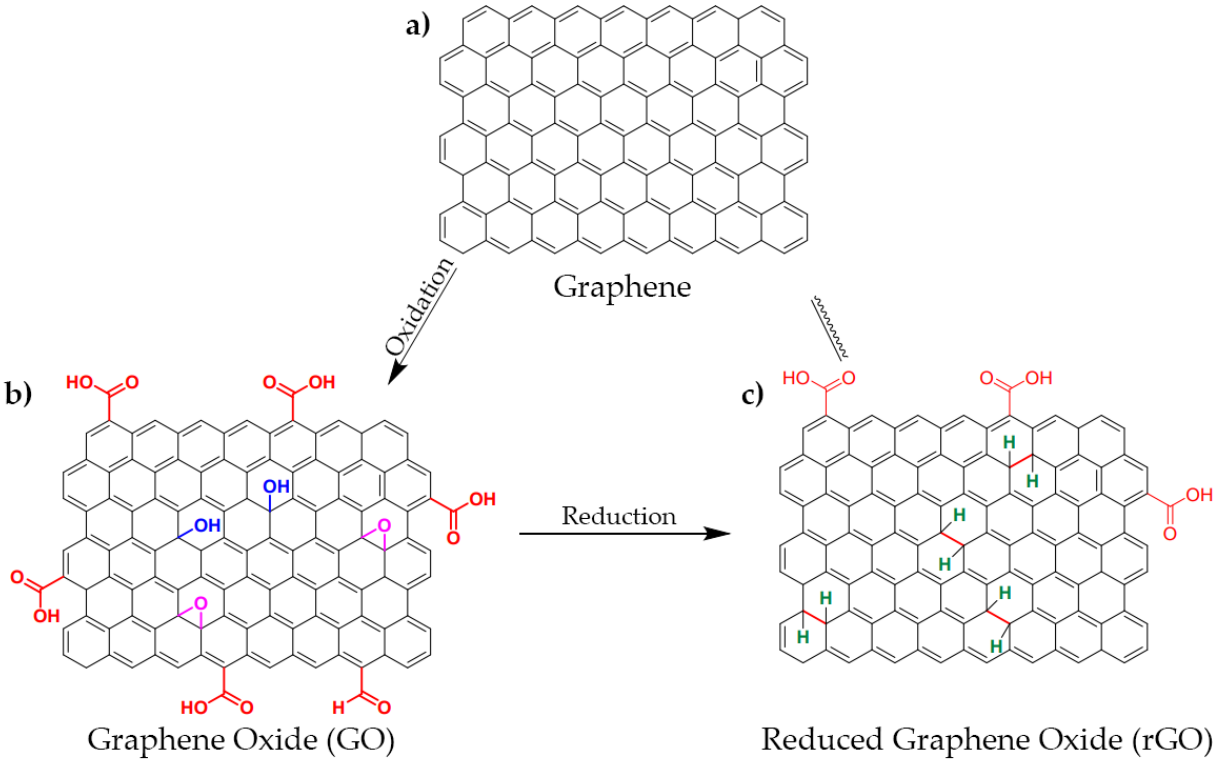

Figure 1.1: *Structural model of: a) single-layer graphene, b) graphene oxide, and c) reduced graphene oxide. Adapted from [18].*

Although many of the well-known physical characteristics of graphene are affected by the existence of these defects, GO is still a very capable nanomaterial, being strong and flexible, with great thermal and electrical conductivity, making it a great candidate for a variety of applications [19, 20, 21]. It can be obtained through various synthesis methods based on the chemical exfoliation and oxidation of graphite flakes, such as the Hummers

[22, 23] or Marcano-Tour processes [24], which have the advantage of producing large yields for a relatively low cost. By comparison, the Marcano-Tour synthesis pathway produces GO with a greater degree of oxidation and a more regular structure [24]. Subsequently, the obtained GO can be further processed in order to obtain reduced graphene oxide (rGO), which ideally possesses no oxygen functional groups attached to the carbon planes, rendering it closer to graphene, the parent nanomaterial [25].

One of the main advantages of using GO for coatings is the ease of forming continuous films through self-assembly at the liquid-air interface [26, 27]. Due to its hydrophilic nature, it is fairly easy to obtain films from GO water dispersions, which is a great aid for the fabrication of sensors, membranes, or even electronic devices [28, 29, 30, 31].

As a coating material, GO has been successfully used on metal substrates, where it showcased good corrosion inhibition [32, 33, 34] and better antimicrobial and biocide effects when compared with conventional polymer alternatives [35]. This is due to the presence of the oxygen functionalities which can induce oxidative stress [36, 37], thus interacting with the nearby chemical substances and biological entities, being of paramount importance for the corrosion and antimicrobial protection [33, 38, 39].

Currently, there are only a handful of studies discussing the potential use of GO as a coating for stone cultural heritage, which showcased its great effectiveness in protecting the stone against erosion and the lack of leaching in the environment, even after heavy rain simulations [40, 41, 42]. There are, however, no studies at the moment that address the changes a GO coating might induce on the stone substrate characteristics, such as modifying water vapour permeability or water capillary absorption, or discussing the physio-chemical interactions underlying the interaction of the nanomaterial with the surface of the stone.

As mentioned before, in discussing the possibility of using GO as a coating for cultural heritage applications, the nanotoxicity and environmental impact of GO are also subjects that have to be addressed. So far, results indicate that the health impact greatly depends on the lateral size, concentration and the degree of oxidation of the nanomaterial [43, 44], with results generally showing a higher risk caused by sheets with a smaller lateral size. Some results indicate the reversibility of the nanotoxicity once the exposure to GO is removed [45, 46], but due to the heterogeneity of GO structures obtained, it might prove difficult to offer general guidelines and conclusions on the health and environmental risks associated with GO usage [44, 47]. It might be better to investigate these risks once a viable GO treatment for stone cultural heritage would be found. Besides the associated health risks, the environmental impact of GO production was recently shown to be low enough so that up-scale to a large scale production would be feasible [48], indicating that the production costs associated to using GO for stone cultural heritage applications might not be an impediment in the future.

We have performed a comprehensive study of employing GO as a protective coating for stone cultural heritage. Given the large influence the synthesis method can have on

the surface characteristics of GO, we also thought on the necessity of performing quantitative dispersability tests of as-prepared GO and a further refined GO fraction with great self-assembly performances at liquid-air interface, in order to fully characterise the potential use of our GO synthesis method for this type of application [27]. Thus, we analyzed the dispersability of both GO types in two of the most popular solvents used for protective coatings for stone materials: water and absolute ethanol, as well as mixtures of both. On the basis of Hansen solubility theory, we also managed to estimate the Hansen solubility parameters of both as-prepared GO and the further refined fraction, information that can be used for choosing a different solvent mixture, while maintaining the stability of the dispersions. We also concluded that, following the refining process, the yield of the improved GO fraction can also be maximized by using a specific mixture of water and absolute ethanol as solvent (40% water and 60% absolute ethanol, by volume), corresponding to the mixture with the best dispersion capabilities.

Then, we investigated the performance of GO as a protective coating for two types of stone with a long history of being used in buildings, statuary complexes or as pavement in North East Italy, namely the Vicenza stone and the Euganean trachyte. During our preliminary tests, we noticed that, against our expectations, the improved GO fraction performed worse than the as-produced GO, since its colour was subjected to a fast darkening process when compared to the regular GO. In addition to this, while brushing, the improved GO fraction tended to thicken, with a consistence similar to a gel, most probably due to a combination of its improved self-assembling properties and the faster evaporation of the absolute ethanol, which consisted of 60% of the solvent's volume. Ultimately, we chose to continue our study on the as-produced GO coatings.

To simulate the impact of weathering on our fresh stone samples, we subjected them to an artificial ageing process, according to existing literature [49], and performed all of the investigations on both natural and the aged samples. We performed analysis on the water vapour permeability, water capillary absorption, water contact angle and colour change before and after the application of the GO coating, in accordance to existing European standards for cultural heritage applications.

In order to simulate the ageing of the GO coating, we then exposed the samples to UV light, and performed the tests again. Investigations were also performed to identify the type of interaction of GO with the stone substrates. In the end, we offer a comprehensive picture on the possibility of using GO as a protective coating for stone cultural heritage, with information both of its protective efficacy, as well as on the most relevant synthesis parameters which affect its surface characteristics.

With the exception of SEM imaging on self-assembled GO films and MIP and XRD analysis on stone samples, all investigations and data analysis was performed by stud. Codruț Costinaș, under the supervision of prof. dr. Lucian Baia. GO synthesis was performed with the aid of drd. Cătălin Sălăgean and lect. dr. Cosmin Coteț. Experimental analysis was done in the laboratories of ICDI-SNA and ICI-BNS research institutes

of Babeș-Bolyai University Cluj-Napoca, as well as in the laboratory of CNR-ICMATE Padova, under the supervision of dr. Patrizia Tomasin, during a six month Erasmus placement mobility. On the subject of GO dispersions, a study regarding their stability in time was recently published by the author [1]. The GO dispersability investigations performed here are the continuation of that study.

[1] C. Costinas et al., "Insights into the Stability of Graphene Oxide Aqueous Dispersions," Nanomaterials, vol. 12, no. 24. MDPI AG, p. 4489, Dec. 19, 2022. doi: 10.3390/nano12244489

Chapter 2

Materials and methods

2.1 Methodology

In investigating the performance of GO as a protective coating for stone cultural heritage, it is of great interest to discuss the influence of the synthesis pathway, which can also be tuned according to needs. Given the emphasis on the formation of homogeneous, uniform coatings, we can assume that maximizing the self-assembly effect would improve the coating's protective efficiency. On this subject, we have noticed earlier that a GO fraction with great self-assembly capabilities (which will be referred to as GO-OL) can be further refined from the product of our original synthesis pathway, which is based on the Marcano-Tour process [27]. Figure 2.1 consists of a schematic representation of the project, offering a clearer picture on how each GO dispersion was obtained. The methods used for the characterisation of the dispersability and stone coatings will be detailed in the following sections.

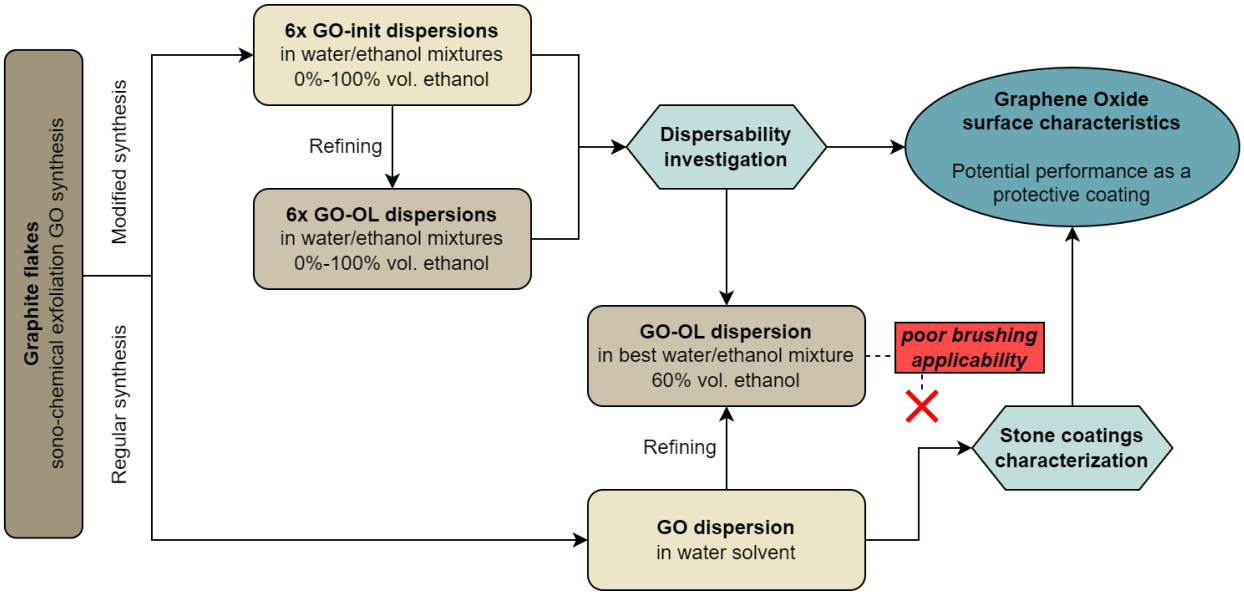

Figure 2.1: *Schematic representation of the project, with the steps taken to provide an overview of the surface characteristics and the potential performance of GO coatings for stone cultural heritage.*

Thus, we have tried to characterize the dispersability of as-produced GO (referred to as GO-init) and GO-OL in two of the most used solvents for the application of protective coatings, namely water and absolute ethanol, as well as maximizing the GO-OL yield from the refining process. Knowing this, different wet chemical functionalization schemes may be later employed successfully in order to modify the surface properties, or for processing the GO dispersions into coatings, thin films, or other composites, using techniques such as spray-coating, solution blending, or others.

The dispersability of both types of GO in water and ethanol was quantitatively characterized through a method based on solvent surface energies and their Hansen solubility parameters [50]. We performed a modified GO synthesis, which resulted in six GO-init dispersions in water, absolute ethanol, and binary solvent mixtures of water and ethanol, with different amounts of ethanol (20%, 40%, 60%, and 80% ethanol). For convenience, the six dispersions were discriminated by the amount of ethanol in the solvent (0%, 20%, 40%, 60%, 80%, and 100%). All six dispersions were subjected to the refining process in order to obtain the target GO-OL fractions, which were also dispersed in the same solvent mixtures. In total, the twelve GO-init and GO-OL dispersions were analyzed through UV-VIS absorption investigations to determine the amount of GO-init or GO-OL left in the supernatant after 2 hours of ultrasonication and 1 hour of centrifugation.

The larger the amount, the better the dispersability of the respective GO material in the solvent of choice. On the basis of "like dissolves like" principle, we were able to approximate the Hansen solubility parameters of both GO-init and GO-OL, as the best performing solvent's parameters, on the basis on the Hansen solubility theory [51]. Both GO-init and GO-OL dispersions were analyzed through DLS and Zeta Potential measurements, and further physio-chemical and surface investigations through XRD, SEM, ATR-FTIR, and Raman spectroscopy on dried self-assembled films, with the goal of understanding the influence of the mixing enthalpy can have on the resulting films.

Then, we tested GO as a protective coating for natural and artificially aged stone samples of Euganean trachyte and Vicenza stone, used in cultural heritage monuments. The regular synthesis pathway was employed for the GO production, and the coatings were applied through the brushing method. In the preliminary trials, we also performed brushing tests with a GO-OL fraction we refined from the GO material, but due to its poor performance we chose to continue with the GO-init coatings. Coating performance has been analyzed on the basis of the specific requirements of coatings to be applied in cultural heritage applications, through its influence on the stone interaction with water (vapour permeability, capillary absorption, and contact angle measurements), as well as aesthetic properties through colorimetry tests. Spectroscopic and surface investigations have also been performed in order to understand the interaction mechanisms of GO with the stone substrate.

2.2 Stone samples

Stone materials differ in their composition (e.g., carbonate, silicate), geological origin (e.g., sedimentary, igneous, metamorphic), and textural features (e.g., porosity, grain size, stratification, etc.) which all affect their bulk behavior against degradation mechanisms [52, 53]. To characterise the efficiency of a protective coating for stone cultural heritage, it is necessary, if possible, to evaluate its performance on a wide range of stone materials.

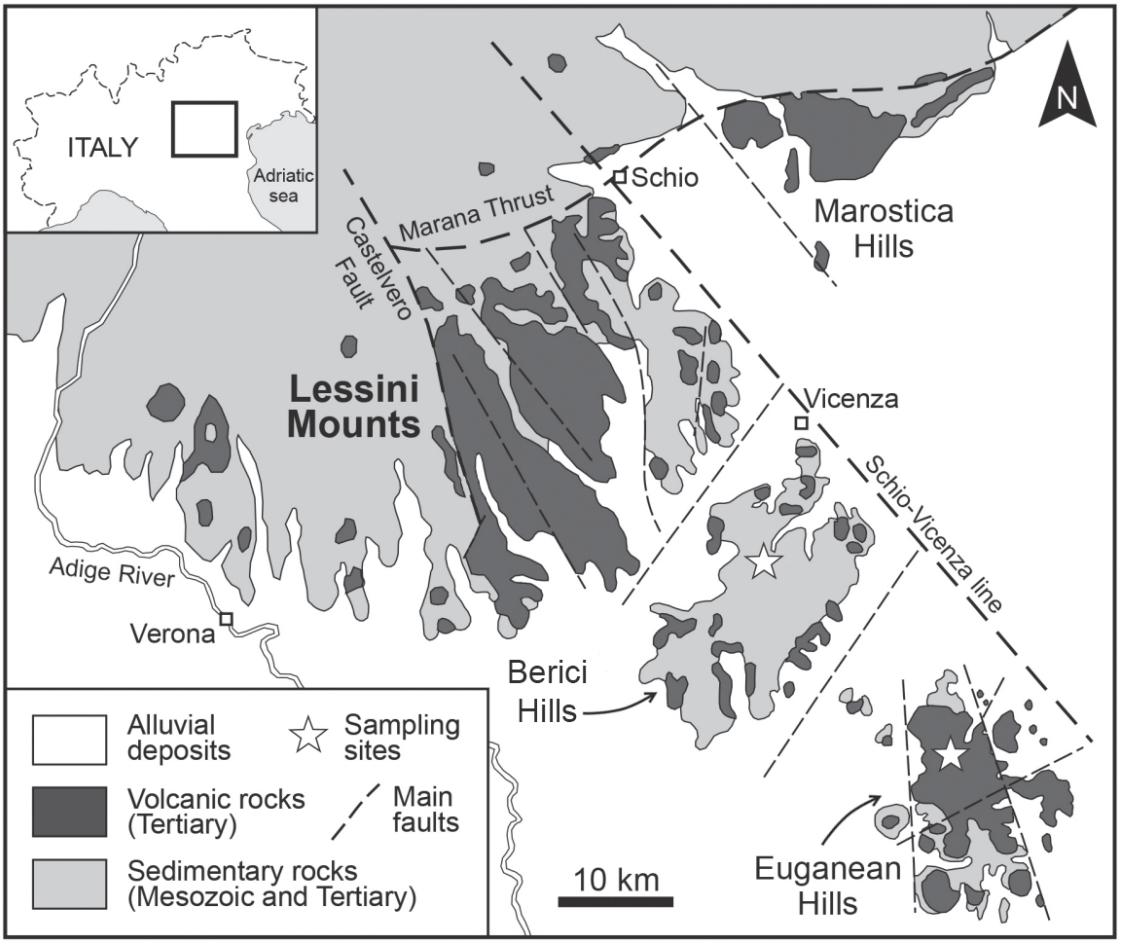

Figure 2.2: *Simplified geological map of the areas around Berici and Euganean Hills, from which the Vicenza stone and Euganean trachyte stone are respectively quarried. Adapted from [54].*

We have chosen to work with two types of stones, namely the carbonatic Vicenza stone and silicatic Euganean trachyte stone, due to their different composition and geological origin, as well as textural features, in order to cover a larger array of the particularities of stone (Figure 2.2). Both types of stones are extracted from the active quarries in North East Italy, in the Berici and Euganean Hills, respectively, and have historically been employed as dimension stones or in the construction of sculptural complexes not far from their point of extraction since Antiquity.

2.2.1 Vicenza stone

Vicenza stone creation dates back to the Middle Eocene and following Oligocene (between 55 and 23 million years ago), and it is a member of the Castelgomberto calcarenite family, one of the fundamental building blocks of Vicenza's Berici hills [55]. It was formed by the buildup of sand, plant fragments and shells at the bottom of a sea that once covered the area where the hills are located now. Several variations of Vicenza stone can be identified, based on the colour, grain, and quarry location, such as the white Costozza variation, or the yellowish-brown Nanto variation [53]. Gray variations can also be found.

From a petrographical point of view, Vicenza stone is an organogenic limestone that is distinguished by a high level of porosity and the inclusion of micro- and macroclastics of foraminifera, bryozoans, algae, and echinoderm [55, 56]. It has an exceedingly heterogeneous structure due to its composition, which is comprised mostly of calcium carbonate (above 90%) with trace amounts of silicon, aluminium, and iron oxides. Physically, it has poor mechanical properties but acceptable workability due to its high compositional heterogeneity and low hardness value. Furthermore, because this stone does not respond well to mechanical stress, due to its low tensile strength, flexion, and compression values, it was mostly used for sculpture and surface fabrication. As a result, it is regarded as a soft stone that may be easily shaped to meet specific requirements.

Vicenza Stone is prone to deterioration due to its high specific surface dictated by porosity and the presence of thin clay layers containing swelling micas such as montmorillonite [56]. The characteristic weathering forms include dissolution and pulverisation (Figure 2.3), which are commonly accompanied by biological colonisation [53]. Vicenza stone has been historically used in numerous complexes around the Vicenza area, both as masonry and in statuary, such as in the Palladian villas (Vicenza, Italy) and for the 78 statues in the square of Prato della Valle (Padua, Italy), exemplified in Figure 2.3.

Figure 2.3: *Left: Typical dissolution and biological colonisation of limestone, to which the Vicenza stone is also subjected. Right: Statuary complex of Prato della Valle, Padua, consisting of 78 statues.*

For our experiments we used samples of the white variation of Vicenza stone, from the Badia quarry. The stone samples were gratefully provided by Fratelli Nichele SRL, Val Liona (VI), Veneto, Italy.

2.2.2 Euganean trachyte

The Euganean Hills are a group of hills in northeastern Italy, entirely surrounded by the Venetian Plain. They were formed in a sub-marine out-welling of basaltic lava during the Eocene, which was followed in the Oligocene by an episode of activity characterized by viscous magma, which formed large deposits of rhyolites and trachytes with moderate alkali metal affinity, while latites and basalts were seldom formed [57]. Euganean trachyte is a denomination that comprises the trachytes, quartz-trachytes, and less common rhyolites and trachyandesites extracted from the Euganean Hills, having in common a characteristic porphyritic texture and gray color, sometimes ranging to brown and yellow shades [58]. Depending on the extraction cave, several different Euganean trachyte varieties can be identified that, although they might belong to the same quarry basin, exhibit a relatively wide array of mechanical performance, strongly depending on their pore characteristics.

From a petrographical point of view, Euganean trachyte is considered a type of igneous rock, with a characteristic fine-grained matrix (a characteristic of volcanic stones). Its chemical composition consists of a large amount of SiO_2 (around 60-65%), with important contributions from Al_2O_3 (around 17%), alkali oxides (Na_2O and K_2O, about 5% each) and lower amounts of Fe_2O_3, MgO, and CaO [58], highlighting its large degree of heterogeneity. Generally speaking, the Euganean trachyte is characterized by good durability and mechanical properties, and a particularly high resistance to abrasion - higher than that of many marbles, sandstones, or limestones, and, in some cases, also comparable to a number of granites - which is one of the reasons why the Euganean Hills have been exploited since pre-historic times [59].

Having good mechanical properties, Euganean trachyte degradation mechanisms are generally dependent on pollutant exposure, resulting in distinctive decay traits such as contour scaling, flaking, and exfoliation, which leads to granular disintegration and crumbling. In the presence of SO_2, black crust forms are also common (Figure 2.4), which are prone to separation and structural damage [60]. Due to its exceptionally good durability and abrasion resistance, Euganean trachyte has been historically used in northern and central Italy as a building material for churches, defensive walls, pavements, such as the pavement of San Marco square in Venice, Italy (Figure 2.4).

In our study we used samples of Euganean trachyte from the Montemerlo quarry, which were gratefully provided by Cave Montemerlo SRL, Cervarese Santa Croce (PD), Veneto, Italy. The Montemerlo quarry is one of the last quarries still active in the extraction of Euganean trachyte, a large share of the stones extracted here being used in the reparation of stone cultural heritage monuments.

Figure 2.4: *Left: Typical disintegration and flaking of trachyte stone [60]. Right: San Marco square, Venice, a world renowned symbol paved with Euganean trachyte.*

2.3 Graphene oxide synthesis

In order to discuss the surface characteristics of GO and its performance as a protective coating for stone cultural heritage, two syntheses of GO have been prepared, which will be detailed in the following sections. A regular synthesis (Section 2.3.1) was used for preparing a GO water dispersion to be used for the protective coatings. A second, modified synthesis (Section 2.3.2) was also made in order to produce six GO dispersions (referred to as GO-init) in water, absolute ethanol, and intermediary binary solvents of water and absolute ethanol, with 20%, 40%, 60%, and 80% of the solvent mixtures composed of absolute ethanol. A fractionation process was further performed on each of the GO-init dispersions, with the goal of obtaining GO fractions with improved self-assembly capabilities. Due to their oil-like consistency, they will be referred to as GO-OL.

For the sake of convenience, the resulting GO dispersions of the modified synthesis will be differentiated by the absolute ethanol volume percentages in the solvent (0%, 20%, 40%, 60%, 80%, and 100% ethanol GO dispersions) and by the type of GO (GO-init or GO-OL). Thus, we can classify the GO dispersions produced for this study as the following:

1. *GO water dispersion.* Produced through the regular synthesis process. Further refining (according to Section 2.3.2) was also done on a portion of this dispersion, for the preliminary tests of GO-OL as a protective coating for stone material.

2. *GO-init water/ethanol dispersions.* Six dispersions, the direct result of the modified synthesis. Each dispersion was composed of GO-init and a mixture of water and absolute ethanol (0%-100% ethanol). After being analyzed, they were subjected to the fractionation process.

3. *GO-OL water/ethanol dispersions.* Six dispersions resulting from the fractionation process of the GO-init dispersions. GO-OL represents the target fraction with better

self-assembly capabilities. Dispersed in the same solvent mixtures of water and absolute ethanol.

2.3.1 Sono-chemical exfoliation

For the synthesis of GO, a sono-chemical exfoliation method was employed, using the primary raw reagents (i.e., graphite flakes, H_2SO_4, H_3PO_4, $KMnO_4$, and H_2O_2) and ratios of the Marcano-Tour process [24]. Our synthesis method includes additional steps of ultrasonication, washing, centrifugation and decantation, and was used before in the production of GO with exceptional self-assembly properties [27, 61].

For obtaining the necessary GO to be used for the protective stone coatings, the synthesis pathway with no additional modifications was used. It can be divided in three steps, outlined in Figure 2.5.

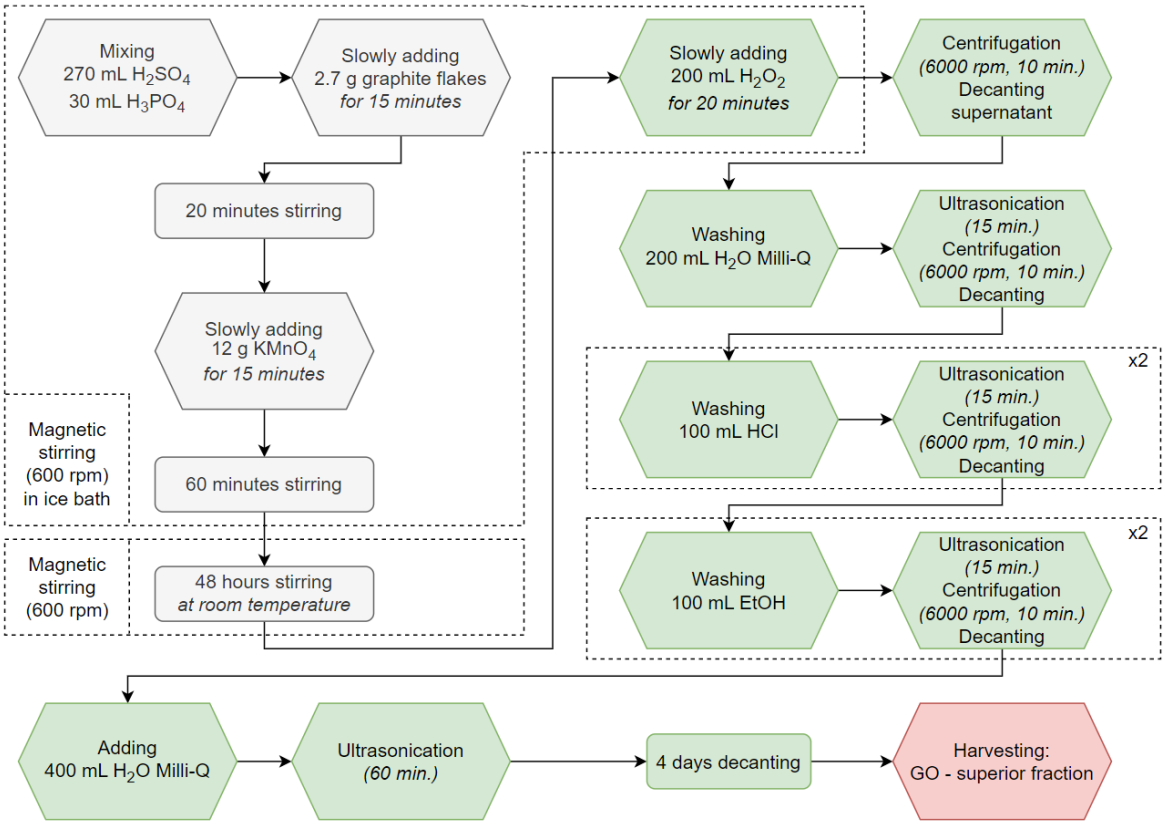

Figure 2.5: *Schematic representation of the regular synthesis process. Adapted from [61].*

In the first step, 270 mL of H_2SO_4 (97%, Nordic Invest SRL, Cluj-Napoca, Romania) and 30 mL of H_3PO_4 (85%, Sigma Aldrich, St. Louis, MI, USA) were mixed in a 9:1 ratio. After 5 minutes, 2.7 g of graphite (99.9995%, powder, 100 mesh diameter, Alfa Aesar, Haverhill, MA, USA) was added in small portions for 20 minutes (i.e., a fifth of the total quantity at a time, with 3 minutes between them) under continuous mixture in an ice bath. Then, 12 g of $KMnO_4$ (99%, Sigma Aldrich, St. Louis, MI, USA) were added in small portions for 15 minutes, while maintaining a continuous mixture and the ice bath. The

initial mixture was then left for 60 minutes under stirring, in an ice bath. Then, the ice bath was removed, and the mixture was left for 48 hours at room temperature, in ambient atmosphere.

The second step of the synthesis method consisted of slowly adding 200 mL H_2O_2 (3%, precooled, Hipocrate 2000 SRL, Bucharest, Romania) for 20 minutes to the mixture, which was stirred in an ice bath. Then, the mixture is left for another 20 minutes to cool in the ice bath, while stirring. Afterwards, the mixture was centrifuged for 10 minutes at 6000 rpm, and the supernatant was decanted away. Then, the remaining solid underwent successive washings with 200 mL H_2O Milli-Q, 100 mL HCl (35%, Sigma Aldrich, St. Louis, MI, USA), and 100 mL absolute ethanol (SC Nordic Invest SRL, Cluj-Napoca, Romania), in that order. After each washing, the mixture was subjected to a series of 15 min of ultrasonication, 10 min centrifugation at 6000 rpm. The supernatant was decanted away every time. The washings with HCl and absolute ethanol were done twice.

After the last decantation, the remaining solid was mixed with 400 mL H_2O Milli-Q, ultrasonicated for 60 min, and kept in a sealed jar for 4 days. The final step of the synthesis consisted in harvesting with a syringe the superior fraction from the jar, and represented the final product of the synthesis. The inferior fraction (about one fifth of the total amount) consisted of a more viscous GO suspension, which may contain unexfoliated graphite, and was not used.

2.3.2 Refining process

In order to characterize the dispersability of GO, another synthesis was prepared using the same amounts of reagents, but with several modifications:

- After the final ethanol washing, the solid was mixed with a larger amount of absolute ethanol (200 mL, SC Nordic Invest SRL, Cluj-Napoca, Romania) and separated in 6 different containers with equal amounts of mixture. This was done in anticipation of the final ultrasonication and centrifugation steps, through which the final solid GO was obtained before its dispersion in the final solvent of choice.

- Following the last centrifugation mentioned earlier, each solid was dispersed in a mixture of H_2O Milli-Q and absolute ethanol, which have been discriminated by the amount of ethanol in solution (ranging from 0% ethanol to 100% ethanol, with four intermediate mixtures with 20%, 40%, 60%, and 80% ethanol). Each dispersion was then ultrasonicated for 60 minutes and left for 4 days at room temperature.

- The final step of the modified GO synthesis consisted in harvesting the superior fraction from each jar, resulting in six GO dispersions in a binary solvent consisting of different mixtures of H_2O Milli-Q and absolute ethanol. In discussing the surface characteristics of the obtained GO, these GO dispersions will be referred to as the GO-init dispersions.

In order to obtain GO fractions with better self-assembly properties, the six GO-init dispersions were subjected to a fractionation process [27]. Each dispersion was ultrasonicated for 30 minutes and centrifugated at 6000 rpm for 120 min, which resulted in the formation of three fractions arranged vertically inside the container. The first fraction, called GO-paste due to its paste-like consistence, was formed at the bottom of the jar. The middle fraction, with an oil-like consistency, called GO-OL, is the GO fraction of interest with great reported self-assembly capabilities. The supernatant, although transparent, was shown to also contain some amounts of GO, but portrayed no interest for us.

These GO-OL dispersions were then analyzed and the results were compared with that of GO-init. As will be discussed later, this fractionation process was also done on the GO water dispersion obtained through the regular method, during the preliminary tests as a stone coating.

2.4 Characterization methods

Particle size distributions and ζ-potential of GO dispersions (0.25 mg/mL) were investigated using a Malvern Nano ZS90 Zetasizer particle analyser (ICDI-SNA Laboratory, Babeș-Bolyai University, Cluj-Napoca, Romania) equipped with a He-Ne laser (633 nm, 5 mW). Each GO dispersion was analyzed in its respective water and ethanol mixtures. Measurements included five sets of 30 observations done at a scattering angle of 90° and a temperature of 25 °C. The laser attenuation level for each measurement was chosen automatically. Each measurement was done three times, and the results were averaged.

XRD diffractograms on GO-init and GO-OL self-assembled films were obtained by using a Shimadzu XRD-6000 diffractometer (ICI-BNS Laboratory, Babeș-Bolyai University, Cluj-Napoca, Romania), using CuK_α radiation (λ = 1.54 nm) and a Ni filter. The patterns were recorded in the 2Θ range between 5° and 50° with a scan speed of 2°/min.

ATR-FTIR absorption spectra of GO-init and GO-OL films were recorded with a JASCO 6600 spectrometer (ICDI-SNA Laboratory, Babeș-Bolyai University, Cluj-Napoca, Romania) within the range of 700–4000 cm^{-1}, at room temperature, with a spectral resolution of 4 cm^{-1}, using a ZnSe crystal.

SEM and EDX analyses were performed on the GO-init and GO-OL self assembled films using a Hitachi SU8230 cold field emission electron microscope (INCDTIM Laboratory, Cluj-Napoca, Romania), coupled with an Oxford Instruments EDX detector. Measurements were done at 30 kV, a working distance of 14.6-15.3 mm, while the elemental composition was obtained using the AZtec Software.

UV-VIS absorbance measurements of GO-init and GO-OL dispersions were done using a JASCO V-780 UV-Visible/NIR Spectrophotometer (ICDI-SNA Laboratory, Babeș-Bolyai University, Cluj-Napoca, Romania). The spectra were measured in the 200 - 800 nm range, with a 0.5 nm resolution. The background measurements were done on each dispersion's corresponding mixture of water and absolute ethanol. For the dispersabil-

ity tests on the supernatant resulted from centrifugation, measurements were done three times at the same wavelength (λ = 235 nm), and the results were averaged.

A Renishaw InVia Reflex Raman spectrometer (Faculty of Physics, Babeș-Bolyai University, Cluj-Napoca, Romania) with an air-cooled RenCam CCD detector was used to capture Raman spectra. For the GO-init and GO-OL self-assembled films, the excitation source used was a 532 nm laser line, with a power of 200 mW. A 30 s exposure duration at 0.1% power was used. For each film, three spectra were acquired from different spots, and the calculated I_D/I_G ratios were averaged. In the case of the GO films prepared from the regular synthesis and the subsequent stone coatings, the excitation source used was a 785 nm laser line, with a power of 106 mW. The laser line was changed due to the strong fluorescence signal coming from both types of stones. A 10 s exposure duration at 10% power was used. In all cases, the spectral resolution was 4 cm^{-1}.

A Nicolet Nexus 870 FTIR spectrometer (CNR-ICMATE Laboratory, Padova, Italy) equipped with a DTGS detector was used for the analysis of the stone characterisation and the GO films prepared from the regular synthesis, using the KBr pellet method (1:100 dilution ratio). For each spectrum, 128 scans were acquired in transmission mode in the 400-4000 cm^{-1} range, with a spectral resolution of 4 cm^{-1}.

The structural characterisation of the stone samples was determined via X-ray Diffraction (XRD) performed by means of a Bruker D8 Advance Plus diffractometer (CNR-ICMATE Laboratory, Padova, Italy) operating in a Bragg-Brentano ϑ-ϑ geometry, using CuK_α radiation (λ = 1.54 nm).

To assess the effects of the protective coatings on weathered stones, we subjected a part of the stone samples to an artificial thermal ageing process, which consisted in heating the dried samples to 400 °C for one hour [49]. In order to assess the effect of the thermal treatment on the open porosity of the stone samples, we investigated them through Mercury Intrusion Porosimetry (MIP) through the use of a Thermo Fisher PASCAL porosimeter with a double module - Pascal 140 and Pascal 240 – which operated at pressures of 40 MPa and 200 MPa. This allowed the effective measurement of pores with a diameter between 3.7 nm and 150 µm. The two measurements were performed, combined and processed through the SOLID version 1.4.1 software. The liquid-solid contact angle for the mercury-stone system is 141.3°. For both Vicenza stone and Euganean trachyte, a sample of the natural and aged stone were tested. A colour change was also noticed between the natural and aged samples.

To simulate the weathering of the GO stone coating, we exposed the treated stone surfaces to a UVC lamp (Helios Italquartz low-pressure Hg lamp) with a total power of 25 W. The lamp's power at wavelength λ = 254 nm is 7.5 W, and was placed at a distance of 1 cm from the samples. The exposure time was set to 7 hours, based on preliminary tests.

To investigate the stone surface morphology with and without the GO coating applied, we used an Olympus SZX12 microscope coupled with a digital camera for optical

microscopy pictures, and the FEI Quanta 200F for SEM images (both at CNR-ICMATE Laboratory, Padova, Italy). For SEM, secondary electrons were collected using an E-T detector (10 kV, working distance of 9-10 mm, spot size 3.0-3.5) to create the SEM pictures.

Water vapour permeability (WVP) tests were performed in accordance to the EN 15803:2010 standard for cultural heritage applications in wet cup conditions [62]. Three samples of each type of stone were prepared by preconditioning the stone discs for 70 hours in a desiccator at 23 °C and 50% relative humidity. Then, in each cup 12 g of H_2O and 6 g of KNO_3 were mixed, with the goal of maintaining an internal relative humidity of 93%. The cups were then capped with the stone discs (approximately 5 cm in diameter and 1 cm in thickness), with the treated face towards the inside of the cup, which was then sealed with Parafilm tape. The cups were then left in the desiccator at a temperature of 23 °C and a relative humidity of 50%. Measurements of the cup weight, desiccator temperature, relative humidity, and air pressure were made every 24 hours, until the system reached a steady state, and were done on the same samples before and after treatments (untreated stones, after the GO coating was applied and after the UV exposure of the coating).

Water capillary absorption (WCA) tests were done according to the EN 15801:2009 standard for cultural heritage applications [63]. For each type of stone, three samples (4 cm cubic samples) have been preconditioned for 66 hours in an oven at 60 °C, then left to cool down to ambient temperature. Stones were weighted before the experiment, and then placed in a container with the treated face on top of a 5 mm layer of filter paper soaked with distilled water. The filter paper was kept soaked at all times using a pipette. The experiment was performed at 23 °C. The samples were weighted at regular times after the start of the experiment (more often at the beginning), until the mass change between two consecutive measurements did not exceed 1%. Each measurement consisted in removing the sample from the soaked filter paper, wiping the excess water on the surface using a microfiber cloth, and then weighting it. Samples were analysed before and after each treatment (untreated stones, after the GO coating was applied and after the UV exposure of the coating).

Water contact angle tests were performed in accordance to UNI EN 15802:2009 standard, used in cultural heritage applications [64]. Measurements were done on the same treated face of the three cubic samples used for each type of stone on the WCA tests. The samples were preconditioned for 3 hours in an oven at 60 °C, then left to cool at room temperature. For the experimental setup, a Dino-Lite microscope was used to photograph the 10 µL water drops. For each sample, 15 measurements were made by photographing the drops 10 s after their contact with the surface. The photographs were then analyzed to determine the contact angle, through the DinoCapture 2.0 software, and the results were averaged. Samples were analysed before and after each treatment (untreated stones, after the GO coating was applied and after the UV exposure of the coating).

For the colorimetry tests, a CM-2600d Konica Minolta spectrophotometer was used to

record the reflectance spectra of each sample, collected in the range of 360 - 740 nm, with a 10 nm resolution. The measurements were performed in the CIEL*a*b* colour space, where L* is the lightness and a* and b* are the chromaticity coordinates in the red-green and the yellow-blue direction, respectively. The instrument has an eight-degree viewing angle geometry, with a Xenon lamp diffusion light and a high-resolution monolithic polychromator. For each point analyzed, three measurements were averaged, and were performed in the SCI (specular component included) mode, on the same cubic stone samples also used for the WCA and contact angle measurements. Through the use of a mask, the same five points on the treated face of the samples were analyzed, before and after each treatment (untreated stones, after the GO coating was applied and after the UV exposure of the coating). The results were used to calculate the colour variation ΔE^* between each treatment, according to the equation:

$$\Delta E^* = \sqrt{\Delta L^{*2} + \Delta a^{*2} + \Delta b^{*2}} \tag{2.1}$$

As mentioned in the introductory section, the colour variation induced by the application of a protective coating should not be noticeable. In accordance to the existing literature, a colour variation greater than 3 becomes visible, while a variation greater than 5 is considered unacceptable for cultural heritage [65].

Chapter 3

Results and discussion

3.1 Dispersability of graphene oxide

This section describes the results obtained after the investigation of GO dispersability in a water and ethanol mixture. Work started with a modified synthesis pathway described in Section 2.3.2, through which six different GO-init dispersions have been obtained. Initially, each dispersion had a total volume of 40 mL and similar concentrations of GO (about 19 mg/mL).

In accordance to the refining process described in Section 2.3.2, we used 35 mL of each GO-init dispersion for the fractionation process. Each dispersion yielded different amounts of each fraction, with the 60% ethanol providing a maximum yield of GO-OL (Figure 3.1). From the beginning, it's worth mentioning that throughout this analysis, both the GO-init and GO-OL dispersions in 100% ethanol behaved in a different way than the other dispersions which included water as part of the solvent. Although this was noticed earlier, it appears that absolute ethanol is not able to properly disperse GO, which causes the decantation of the nanomaterial at the bottom of the container, leaving the clear solvent on top. It is the first clue on the importance of the presence of water molecules in the solvent.

The particle size distribution of the GO dispersions of interest (GO-init and the refined GO-OL) have been analyzed (Figure 3.2). In the case of 2D nanosheets such as GO, DLS results are difficult to interpret, due to the fact that the method assumes the radiation is reflected by spherical structures. Thus, the particle size distributions might only be compared in search of large differences, since they cannot provide reliable information on the size of planar structures. It might be possible, however, that the peaks observed have their origin in the well-defined anisotropy of the diffusion coefficient for planar structures [61].

Similarly, ζ-potential distributions have been obtained. The distributions of both GO-init and GO-OL dispersions can be seen in Appendix A1.1, Figure A1.1. The average values are represented in Figure 3.3, in which we can observe that increasing the amount of ethanol in the solvent mixture leads to an increase of the ζ-potential values.

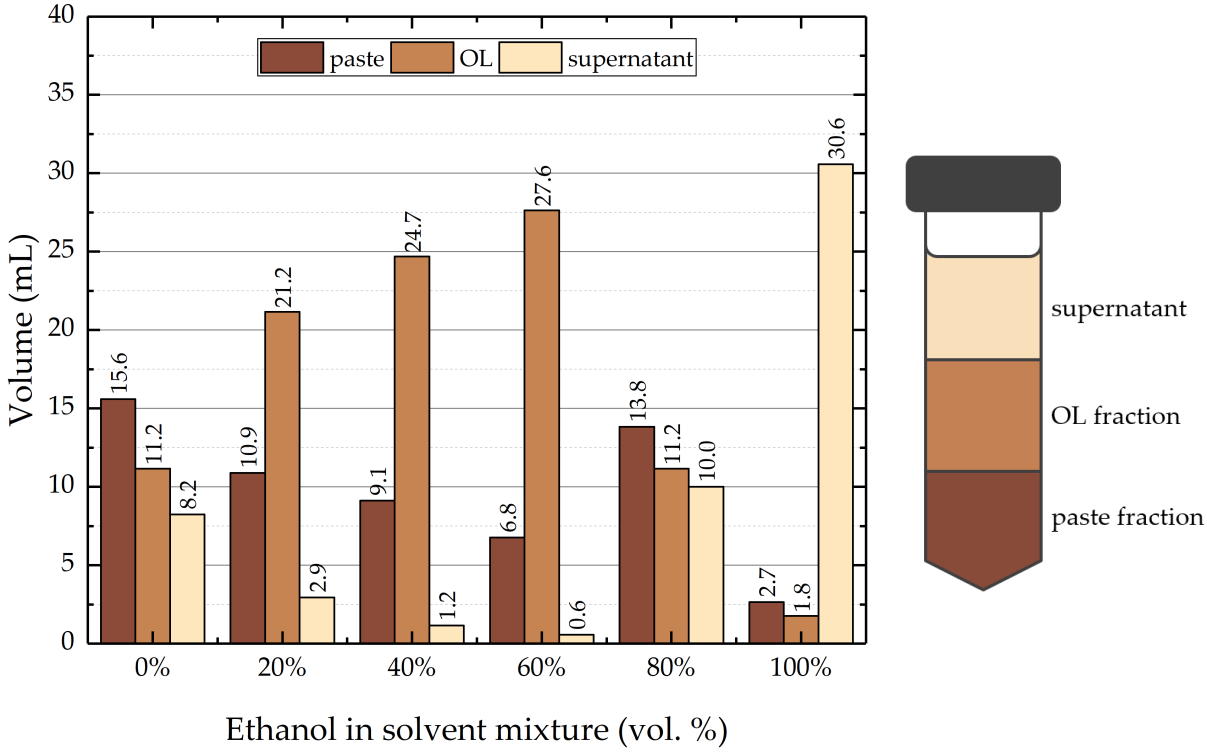

Figure 3.1: *Left: Quantities obtained of each refined GO fractions (paste, OL, and the supernatant). A maximum output can be noticed for the 60% ethanol dispersion, while almost no GO-OL resulted from the 100% ethanol fraction. Right: Vertical arrangement of the paste, OL, and supernatant fractions in the containers after the refining process.*

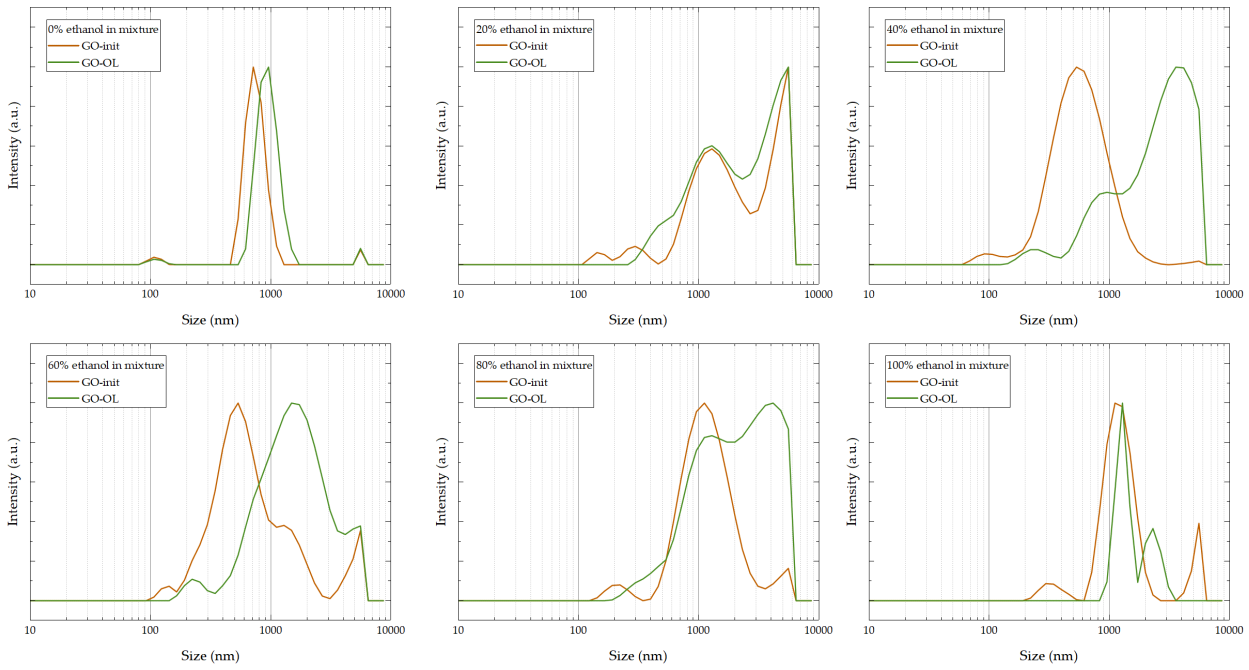

Figure 3.2: *Particle size distributions of GO-init and GO-OL dispersions in their respective water/ethanol mixtures. Generally, we can distinguish three peaks in each distribution. A shift towards larger sizes occurs for the GO-OL fractions.*

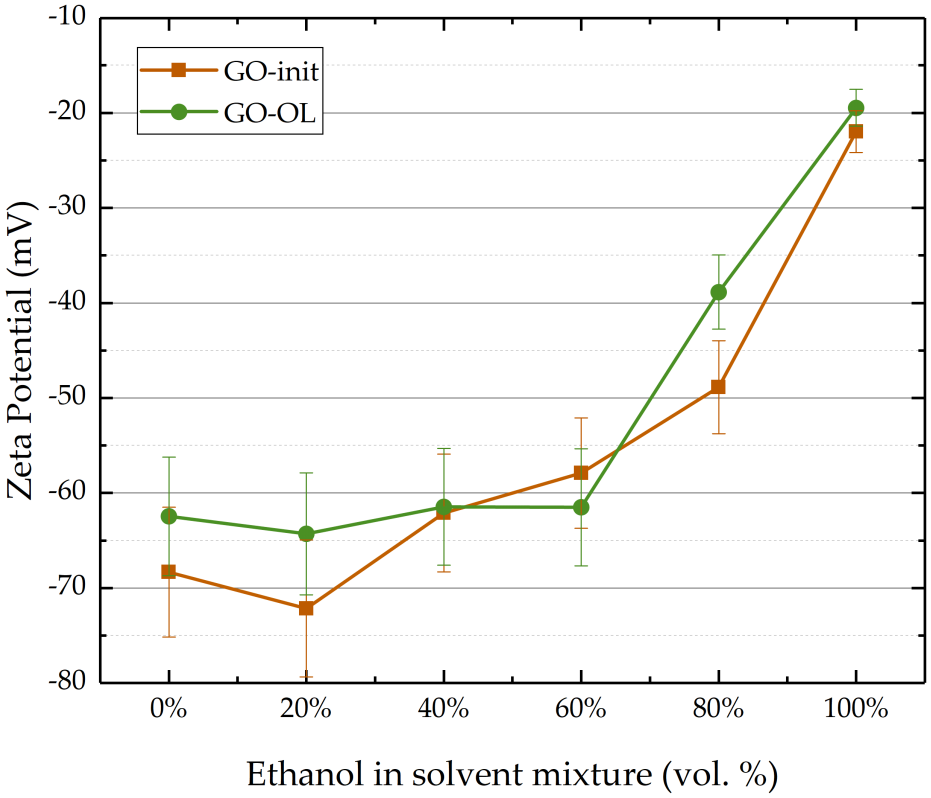

Figure 3.3: *Average ζ-potential values for each GO-init and GO-OL dispersion. An instrumental error of 10% was considered. The lowest values have been obtained for the 20% ethanol GO-init dispersion.*

From each dispersion we took 1 mL and left it to dry on a watch glass for 1 week in ambient conditions. Once placed on the watch-glass, the self-assembly of GO at liquid-air interface started to be noticeable. In the case of GO-init dispersions, the quickest self-assembly occurred for the 40% ethanol dispersion, when compared to the others. Generally, it took several minutes for the films to appear. For GO-OL, however, the quickest films appeared from the 60% ethanol dispersion, and it usually took between 10 seconds to a minute for each GO-OL film to appear. There was no self-assembly effect seen in the 100% ethanol dispersions, and the dried GO-init and GO-OL appeared in powder form, adhered to the glass substrate.

The dried films were then subsequently used for XRD, SEM-EDX, ATR-FTIR, and Raman spectroscopy investigations, in order to identify potential physio-chemical or morphological differences. A comparison on the obtained XRD diffractograms obtained for the self-assembled films of GO-init and GO-OL can be seen in Figure 3.4. The characteristic (001) peak of GO is noticeable at 2Θ values of about 10°, and has been used to compute the interlayer distance, in accordance to Bragg's law (Figure 3.5):

$$n\lambda = 2d \sin \Theta \tag{3.1}$$

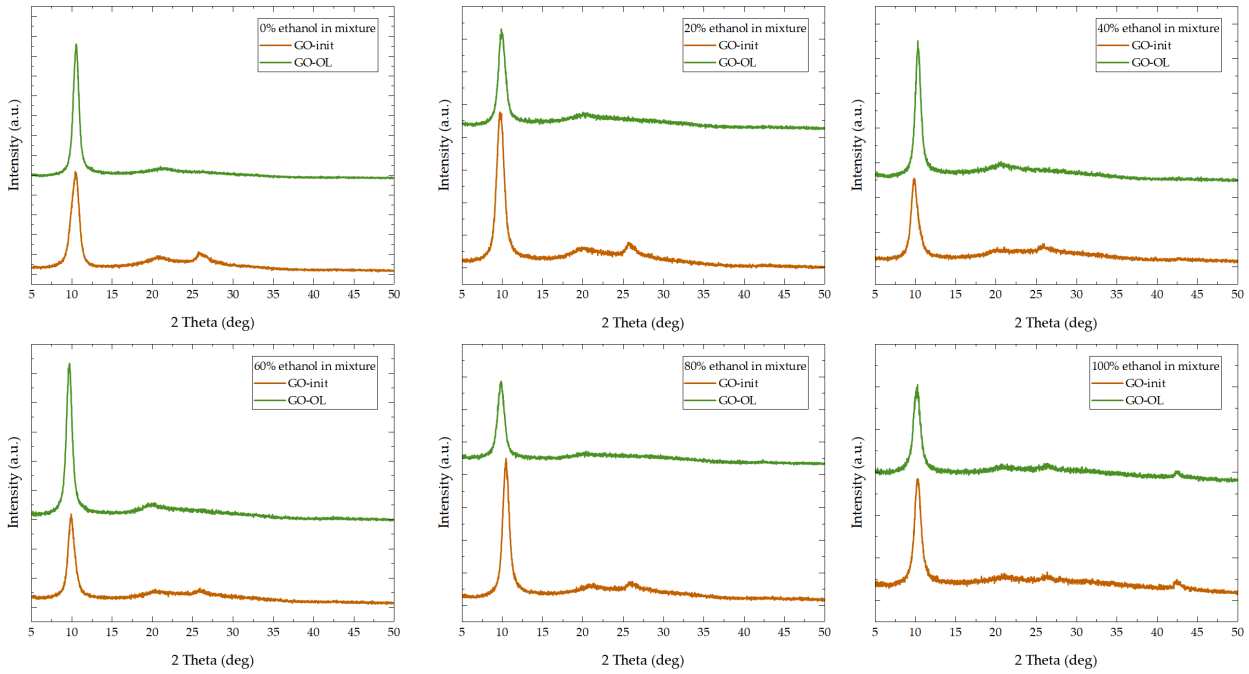

Figure 3.4: *XRD diffractograms of GO-init and GO-OL self-assembled films at the liquid-air interface. Each film was dried in its respective solvent, consisting of water and ethanol mixtures.*

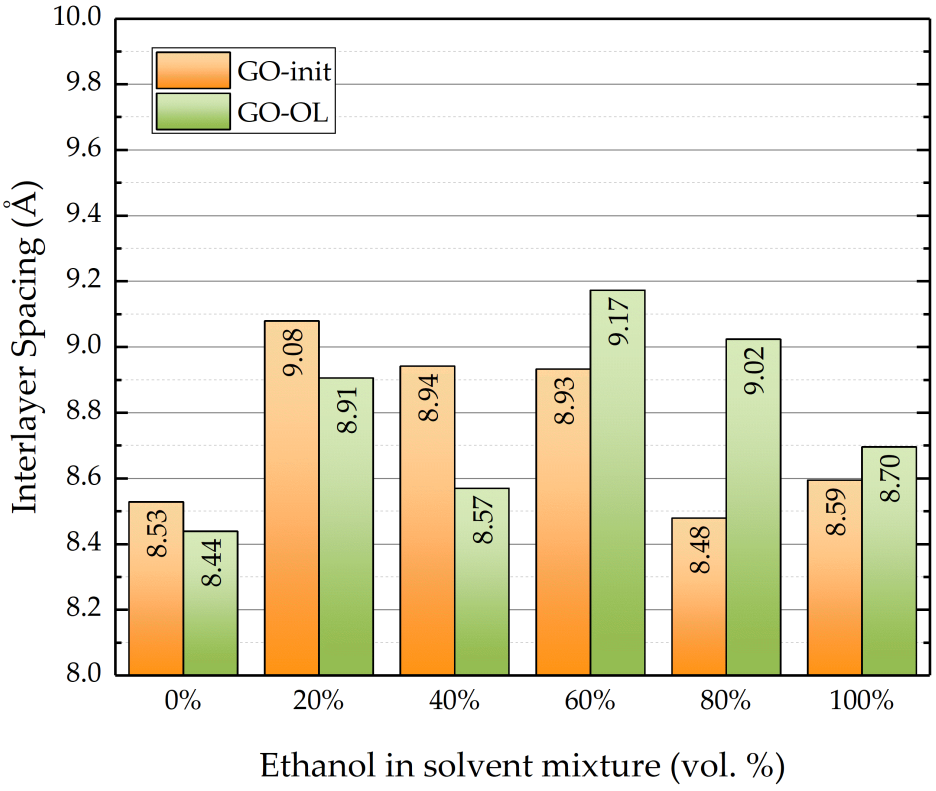

Figure 3.5: *Calculated interlayer distance for each GO-init and GO-OL self-assembled film, on the basis of Bragg's equation. As ethanol molecules begin to penetrate inside the structure, the interlayer distance increases.*

A broad peak of lower intensity can also be seen in all samples at 2Θ values of about

22°, which is characteristic to (002) reflections of leftover graphitic domains. However, the same (002) reflection can also be seen at $2\Theta = 26°$ in GO-init films, for well defined unoxidized graphitic domains, indicating incomplete exfoliation [66]. This is not observed in the case of GO-OL films. Furthermore, in the case of dispersions in 100% ethanol, we can see an additional peak at $2\Theta = 43°$, which is the result of (100) reflections, indicating incomplete exfoliation. Overall, we can observe that by using a solvent mixture richer in ethanol, the crystallinity of GO self-assembled films is slightly decreased, when compared to the water mixture. Furthermore, the GO-OL refined fractions seem to lack well defined graphitic domains, the ones seen for GO-init.

Micro-scale SEM images have been taken to investigate the morphology of each film, and are presented in Appendix A1.2, Figures A1.2 and A1.3. A continuous morphology with folding features can be observed in the case of GO-init and GO-OL films obtained from dispersions containing water, in accordance to the observed self-assembly effects. Dried samples obtained from GO-init and GO-OL in 100% ethanol showcase some continuous aggregates of micrometer size, which agglomerate in larger formations. Debris is also visible, especially for GO-init, while GO-OL showcase a layered type of structure composed of long aggregates.

ATR FT-IR spectra of the obtained films can be seen in Figure 3.6. The characteristic GO absorption bands can be observed, in accordance to the existing literature [66, 67, 68, 69]. Thus, the wide absorption band at about 3420 cm^{-1} appears due to the O-H stretching vibration, the band around 1735 cm^{-1} is given by the C=O stretching vibration, the band around 1640 cm^{-1} is attributed to the stretching vibration of the C=C bonds and the absorption band around 1430 cm^{-1} is assigned to the S=O stretching vibration. The signals recorded in the 1250–1000 cm^{-1} region appear due to the stretching vibrations of the C-OH (about 1220 cm^{-1}), C-O-C (about 1165 cm^{-1}), and C-O bonds (about 1050 cm^{-1}). Overall, there are not many differences observed between the GO-init and GO-OL IR spectra, indicating that both contain the same types of functional groups. Observed differences might arise from the distribution of functional groups on the surface, or through the interaction with solvent molecules.

Raman spectroscopy was further employed in order to obtain additional information on the physio-chemical characteristics of the GO films. Individual Raman spectra for the GO-init and GO-OL samples can be observed in Annex A1.3, Figures A1.4 and A1.5. The characteristic D and G bands of GO are present, while a lower presence of the 2D and other overtone bands is seen, indicating a large degree of oxidation [70, 61]. The I_D/I_G ratio, used to describe the degree of oxidation of GO structures, has also been calculated from the spectra (Figure 3.7). Although a small difference, on average GO-OL samples display a slightly higher I_D/I_G ratio, indicating a relatively larger oxidation degree, when compared to GO-init. It is also relevant to note the lower deviations from the average values obtained for GO-OL samples, when compared to GO-init, which might indicate that a more homogeneous structure was obtained through the further refining process.

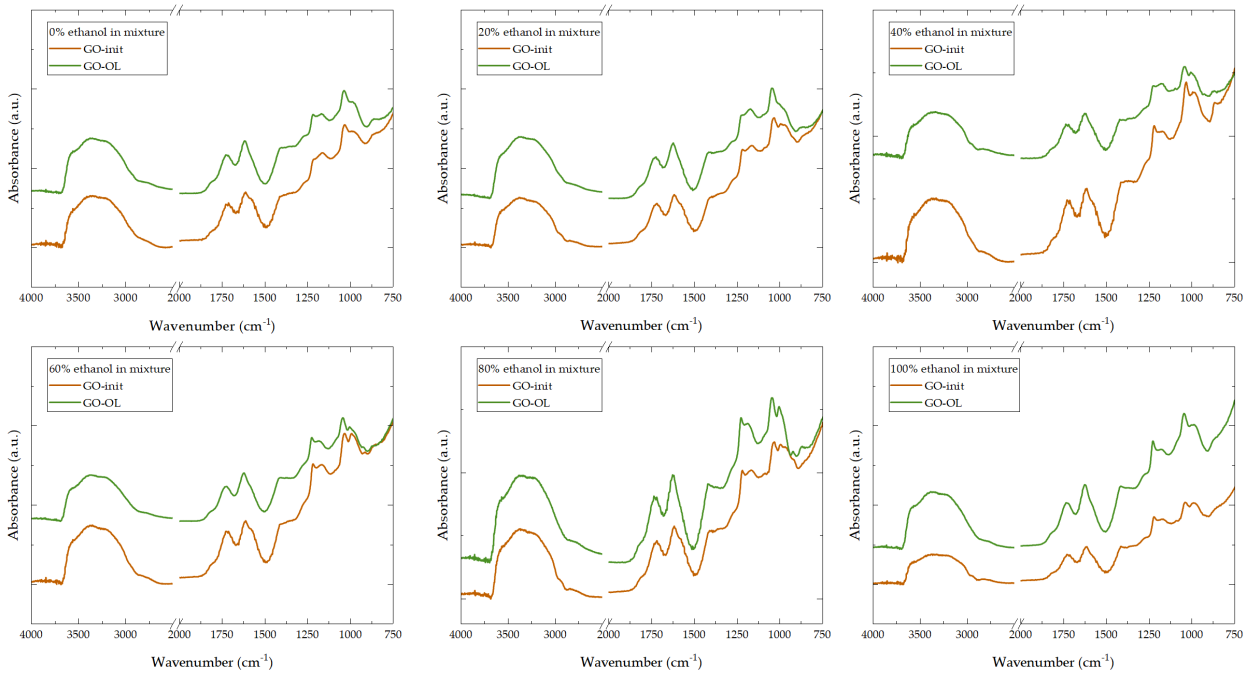

Figure 3.6: *Recorded IR of GO-init and GO-OL self-assembled films at the liquid-air interface. Each film was dried in its respective solvent, consisting of water/ethanol mixtures.*

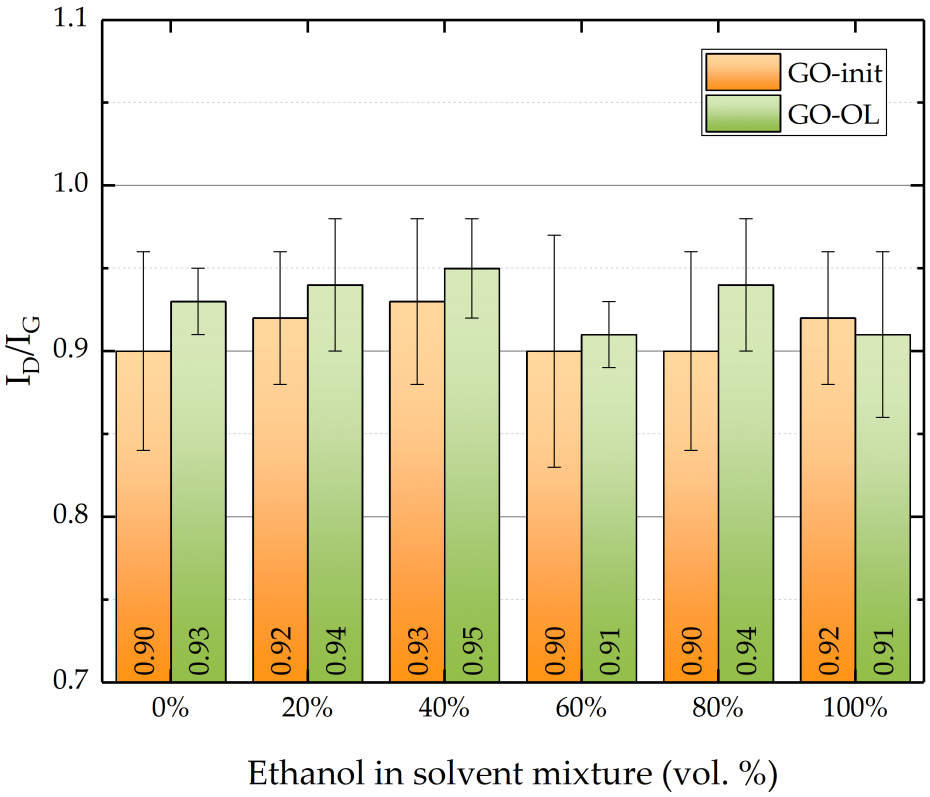

Figure 3.7: *Calculated I_D/I_G ratios for the GO-init and GO-OL samples. Three Raman spectra have been used for each sample. Average values and standard deviations are shown.*

In order to characterise the dispersability of GO in water and ethanol mixtures, we chose a quantitative method based on the Hansen solubility theory of solutes in a sol-

vent [51]. On its basis, the dispersability of a nanomaterial in a solvent is determined by the energetic cost of mixing the two components, and can be evaluated through their corresponding enthalpy of mixing. Since GO can be considered a 2D nanomaterial, the molecular interactions with the solvent molecules take place mostly on the surface of the nanosheets. Thus, the surface energies of the solvent and the nanomaterial will constitute the main components. Ultimately, the energetic cost of mixing the two components is minimized for similar or equal surface energies [50, 51]. This is the physio-chemical basis of the well-known empiric principle of "like dissolves like", and is the foundation of the method we further employed for the characterization of GO dispersability.

A detailed, quantitative analysis of the surface characteristics of GO can be done on the basis of the Hansen solubility parameters, corresponding to the dispersive, polar, and hydrogen-bonding components of the cohesive energy density used to describe the dispersability of GO [50, 51]. Thus, we can write the enthalpy of mixing as:

$$\Delta H_{mix} = \left[\left(\delta_{D,2D} - \delta_{D,sol}\right)^2 + \left(\delta_{P,2D} - \delta_{P,sol}\right)^2 + \left(\delta_{H,2D} - \delta_{H,sol}\right)^2 \right] \phi(1-\phi) \qquad (3.2)$$

where δ_D, δ_P, and δ_H are the dispersive, polar, and hydrogen-bonding Hansen solubility parameters of the 2D nanomaterial or the solvent, and φ is the volume fraction of the 2D solute in the solvent. We can easily notice that ΔH_{mix} is minimized for equal values of the solubility parameters of the 2D solute and the solvent. As a consequence, through empirical observation of the most effective solvent for an unknown solute, one can reliably approximate the Hansen solubility parameters of the nanomaterial as the values corresponding to the parameters of the best solvent.

The modified synthesis we performed yielded six GO-init dispersions in mixtures of water and ethanol. In theory, the Hansen solubility parameters of a mixture are a linear combination of the individual components, weighted by the volume fraction of each component [51]. Thus, we computed δ_D, δ_P, and δ_H for each of the water and ethanol mixtures. The first step of the analysis consisted of investigating the UV-VIS absorption spectra of each GO-init dispersion, at the same concentration (Figure 3.8). The π-π^* transition of the atomic C-C bonds is observed at about 235 nm, while a shoulder peak at about 300 nm assigned to n-π^* transitions is also noticeable. The maximum absorbance occurs at 235 nm for each sample, with the GO-init dispersion in the 60% ethanol mixture showing the largest absorbance. This might be due to the smaller size of the GO-init nanosheets, which have improved absorbance capabilities compared to larger sized GO nanosheets [71].

For the dispersion tests we subjected 20 mL of each GO-init dispersion (0.1 mg/mL) to 2 hours of ultrasonication and 1 hour of centrifugation. Following these steps, each dispersion separated into a supernatant and a decantant. The amount of GO-init retained in the supernatant after ultrasonication and centrifugation was taken as a measure of the ability of the solvent to colloidally stabilize the material. Based on the observed UV-VIS spectra, we chose a working wavelength of 235 nm for estimating the amount of GO in the

supernatant, corresponding to the maximum absorbance peak of GO. We also performed tests to ensure water and ethanol are completely transparent at 235 nm. Ultimately, from the absorbance measurements, we can also compute the concentration of GO-init, in accordance to the Beer-Lambert law:

$$\frac{A}{l} = \alpha C \tag{3.3}$$

where A is the measured absorbance, l is the optical path length, α is the extinction coefficient, and C is the concentration of GO-init.

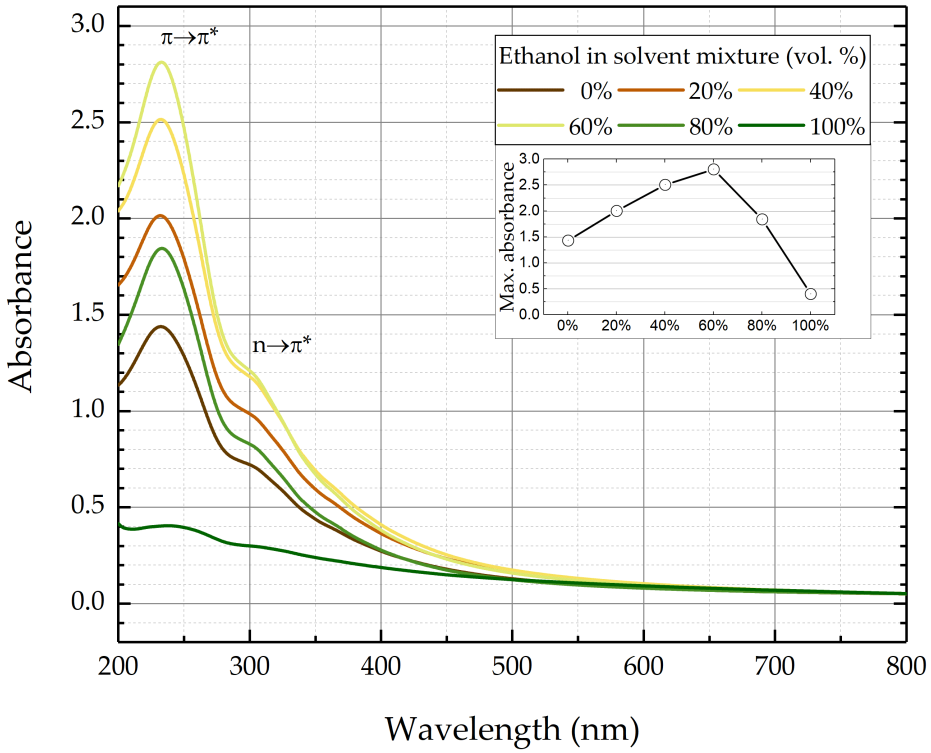

Figure 3.8: *UV-VIS absorption spectra of GO-init dispersions in water and ethanol mixtures. The corresponding water and ethanol mixtures were used for the background scans and were then subtracted.*

The same exact procedure has been followed for the GO-OL dispersions obtained through the subsequent refining process. For each supernatant five measurements have been done, and the average and standard deviation have been provided as a function of the Hansen solubility parameters of each solvent mixture of water and ethanol (Figure 3.9). From the experimental results we can then estimate the Hansen solubility parameters of GO-init and GO-OL as the δ_D, δ_P, and δ_H corresponding to the maximum absorbance per optical path length measured.

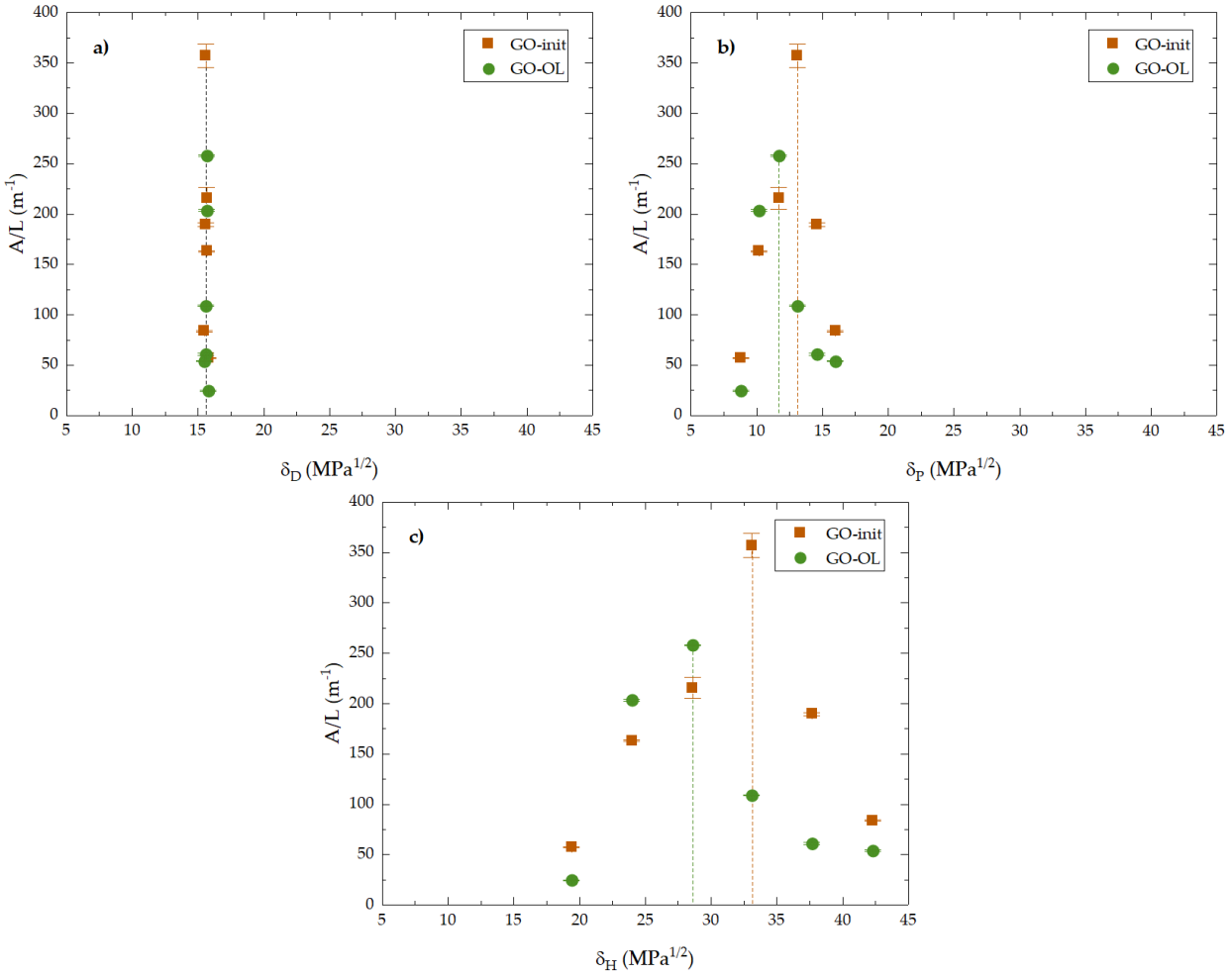

Figure 3.9: *Absorbance per optical path length at 235 nm for GO dispersions following ultrasonication and centrifugation, as a function of a) δ_D, b) δ_P, and c) δ_H of each solvent at 25 °C. Droplines represent the maximum A/l values obtained for GO-init and GO-OL.*

Results are presented in Table 3.1, together with literature values for GO, RGO, pristine graphene, and pristine graphite nanofibers (PGNF). By comparison, little variation is usually seen for δ_D, as generally these types of materials can be easily dispersed by solvents with δ_D values of around 15-18 MPa$^{1/2}$. Slightly larger variations can be noticed for δ_P values, which can be found in the range of about 8-13 MPa$^{1/2}$. By comparison with graphene, it is noticeable that the presence of oxygen functional groups decreased the δ_D and increases the δ_P values. As noticed in our work, the largest distribution can be seen for δ_H values, suggesting that hydrogen-bond interactions between GO and solvent molecules are the most important mechanism in its successful dispersability. Low values of δ_H=7.7 MPa$^{1/2}$ have been reported for pristine graphene, and as the number of oxygen functional groups increases, $_H$ rises to a maximum value of 33.1 MPa$^{1/2}$, for GO-init. As previously suggested [50], it appears that the oxidized domains of GO, rather than pristine domains, dominate the dispersion mechanism.

Table 3.1: *Hansen solubility parameters of GO-init, GO-OL and other types of graphene materials.*

	δ_D $MPa^{1/2}$	δ_P $MPa^{1/2}$	δ_H $MPa^{1/2}$	Ref.
GO-init	15.6	13.1	33.1	This work
GO-OL	15.7	11.7	28.6	This work
GO	17.1	10.0	15.7	[72]
RGO	17.9	7.9	10.1	[72]
RGO	16.9	10.7	14.1	[50]
Graphene	18.0	9.3	7.7	[73]
PGNF	16.4	8.6	14.7	[74]

Maximum dispersability has been achieved for water and ethanol solvent mixtures with 40% ethanol for GO-init, and 60% ethanol for GO-OL, for which a maximum yield was also obtained in the refining process. Lower values for δ_H and δ_P also indicate that GO-OL has slightly lower hydrogen-bond and polar interactions with the solvent than GO-init, possibly due to a slightly lower ratio of oxidized domains. This relates to the observed ζ-potential values for GO-init and GO-OL dispersions, for which more negative values have been noticed for GO-init.

Taking into account all the results discussed so far, it appears that the refining process yields a GO-OL fraction that keeps the same oxygen functionalities as the initial GO, but has no leftover graphitic domains caused by incomplete exfoliation. This leads to an improved self-assembly mechanism, and the formation of GO-OL films with a more homogeneous structure, as noticed in the Raman spectra. As seen in the values obtained for the δ_D, δ_P, and δ_H solubility parameters, it appears that the synthesis pathway and the further refining process is capable of producing a very oxidized type of GO, with great capabilities of forming hydrogen-bonds with surrounding molecules. From a practical point of view, this has further implications, since the surface characteristics of a 2D nanomaterial dominate its behaviour. Choosing the right solvent is crucial for maintaining the stability of the dispersions, and the water and ethanol mixtures formed stable GO dispersions for a long time.

3.2 Performance of graphene oxide as a protective coating

Assessment of the potential use of GO as a protective coating for stone materials started with the analysis of the two different types of stones we chose to use, namely the Euganean trachyte and the Vicenza stone. Since protective coatings in stone cultural heritage are sometimes applied on aged and weathered stones, we chose to perform an artificial ageing process on some of the samples, with the goal of comparing the performance of GO on both types of substrates: natural, fresh quarried stone and artificially aged samples. Transmission FT-IR using the KBr pellet method and XRD analysis has been per-

formed on powdered stone samples (Figures 3.10 and 3.11).

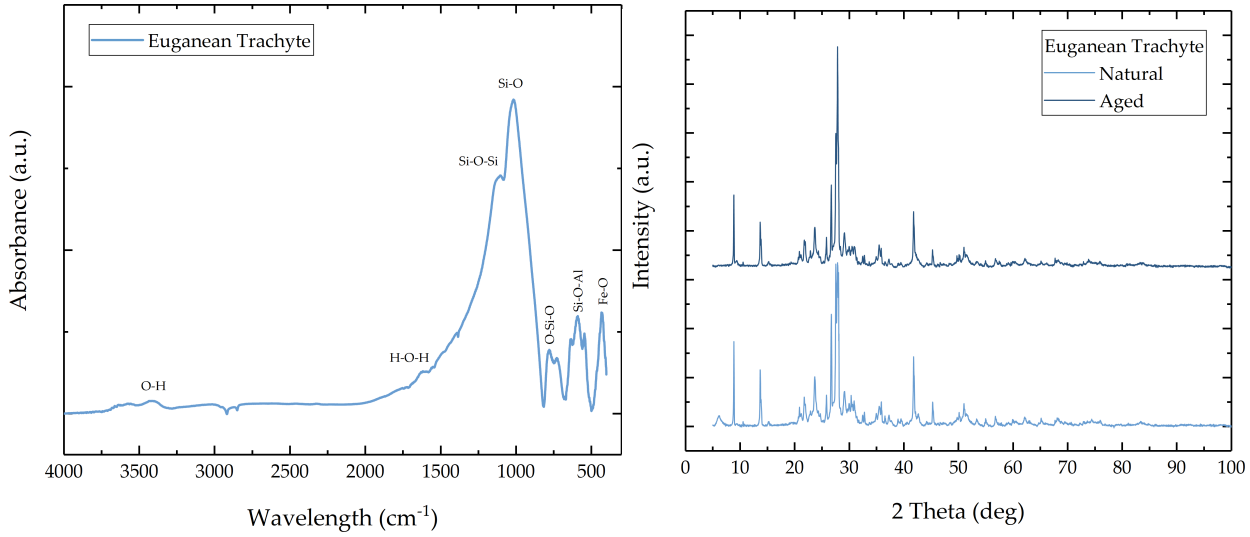

Figure 3.10: *Left: FT-IR absorption spectrum of Euganean trachyte. Right: XRD diffractograms of natural and aged Euganean trachyte.*

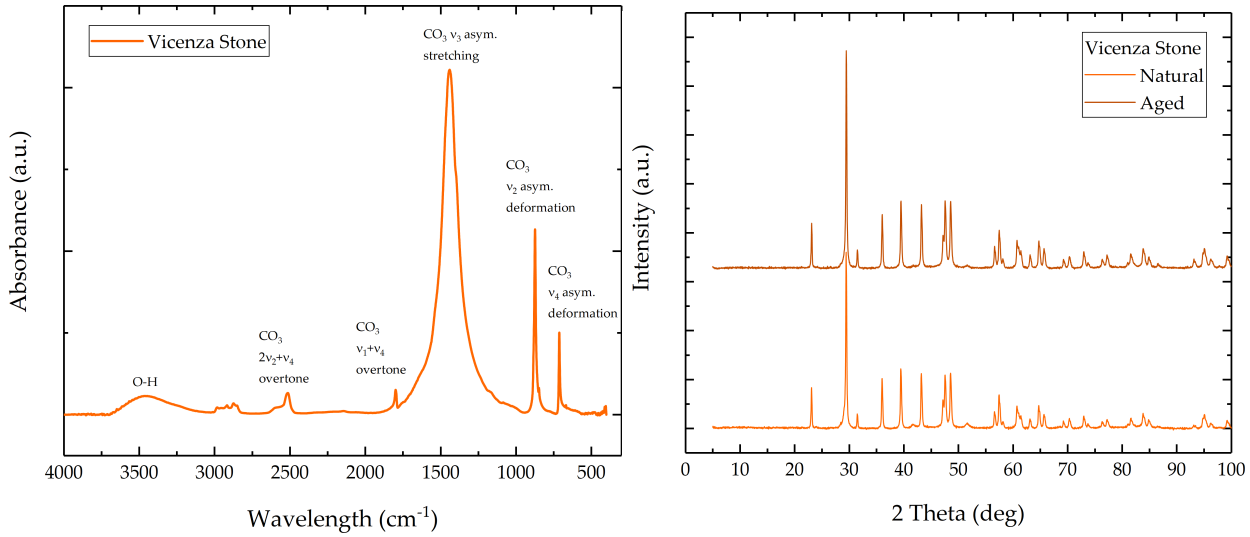

Figure 3.11: *Left: FT-IR absorption spectrum of Vicenza stone. Right: XRD diffractograms of natural and aged Vicenza stone.*

The following absorption bands of Euganean trachyte can be identified in the FT-IR spectrum: the stretching vibration of O-H (about 3400 cm^{-1}), the bending vibration of H-O-H (at about 1630 cm^{-1}), the bending vibration of Si-O-Si (at 1115 cm^{-1}), the stretching vibration of Si-O (at 1015 cm^{-1}), the bending vibration of O-Si-O (at 781 cm^{-1}), Si-O-Al vibration (at 593 cm^{-1}), and a Fe-O vibration (at 430 cm^{-1}) [75]. Little to no difference is observed in the XRD diffractograms of natural and aged Euganean trachyte samples, which exhibit reflections of the main crystal phases present: Albite, Microcline, Muscovite, and Aluminum Diopside [57, 75].

The FT-IR absorption spectrum of Vicenza stone exhibits the well-known IR-active $Ca(CO)_3$ bands: the ν_4 asymmetric deformation (at 712 cm^{-1}), ν_2 asymmetric deformation

(at 873 cm^{-1}), ν_3 asymmetric stretching (at 1440 cm^{-1}), and combination overtones of $\nu_1+\nu_4$ (at 1799 cm^{-1}) and $2\nu_2+\nu_4$ (at 2515 cm^{-1}) of the CO_3 ion, as well as the stretching vibration of O-H (at about 3480 cm^{-1}) [76]. XRD patterns of Vicenza stone exhibit the typical reflections of calcite, and little to no difference can be seen between the natural and aged samples, which exhibit a very good degree of crystallinity [76].

Through MIP tests, we have analyzed the porosity of natural and aged stone samples. Pore size distributions can be observed in Figures 3.12 and 3.13, while the stone densities and porosimetric parameters are presented in Table 3.2. In the case of Euganean trachyte, we first see a unimodal distribution with a peak at about 0.08 µm, which changes to a bimodal distribution following the aging process. A new peak appears at about 2.5 µm, as the thermal treatment cracks the matrix and connects existing pores. For Vicenza stone, the ageing process enhances the relative amounts of 1 µm and 10.5 µm. Overall, the ageing process does not change the overall shape of the pore distributions, but rather generates pores of specific sizes as a result of thermal stress, which collapses pores in the stone matrix [49].

From the analysis discussed earlier, we can define the two types of stone substrates to be further used in investigating the performance of the GO coatings as the following:

- *Euganean trachyte*: a compact silicatic stone substrate with medium open porosity, with numerous impurities of Al, Na, K, Fe, and Mg present in the matrix. Following the artificial ageing process, a new set of samples with different pore size distribution was also prepared.

- *Vicenza stone*: a highly porous carbonatic stone substrate with large open porosity, but a rather homogeneous chemical composition. Further increase of the open porosity was achieved through the artificial ageing process.

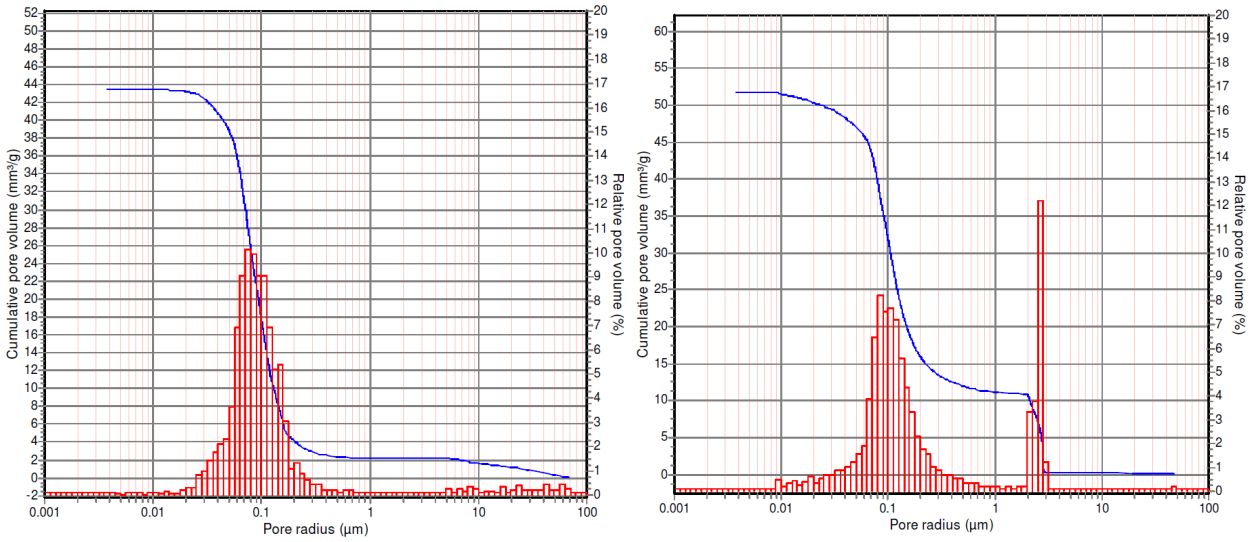

Figure 3.12: *Pore size distributions of natural (left) and aged (right) Euganean trachyte.*

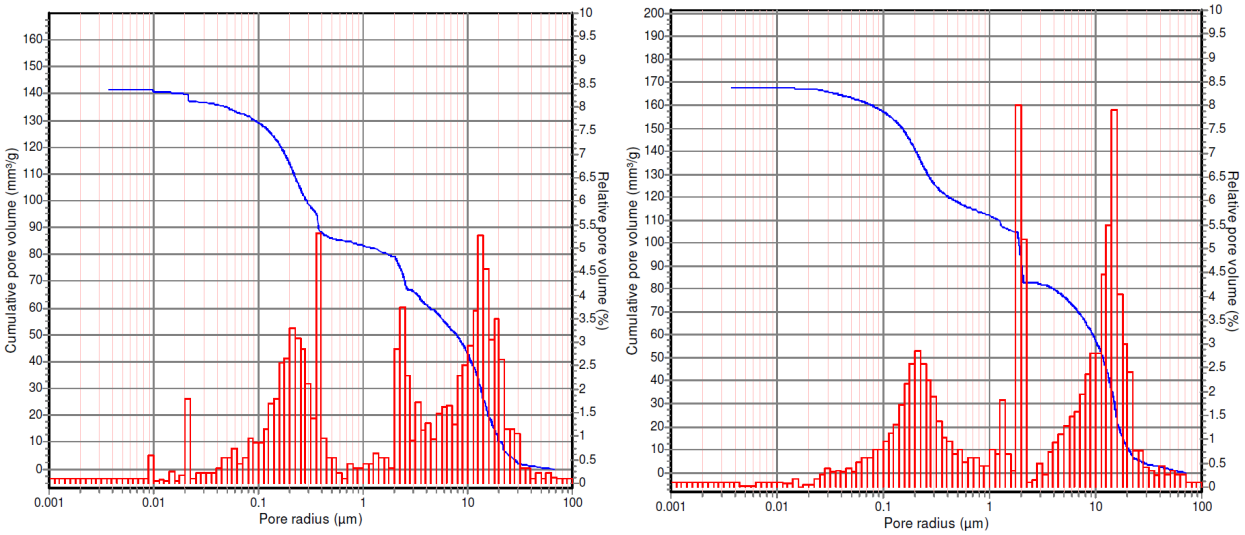

Figure 3.13: *Pore size distributions of natural (left) and aged (right) Vicenza stone.*

Table 3.2: Mean values of density and porosimetric parameters determined by MIP on natural and aged Euganean trachyte and Vicenza stone.

Sample	Bulk density (g/cm^3)	Apparent density (g/cm^3)	Open porosity (vol. %)	Mean pore radius (µm)	Median pore radius (µm)	Total pore volume (mm^3/g)
ET Natural	2.3506	2.6185	10.23	0.0792	0.0888	43.52
ET Aged	2.4154	2.7608	12.51	0.0942	0.1183	51.79
VS Natural	1.8004	2.4167	25.50	0.2216	2.4753	141.63
VS Aged	1.9459	2.8902	32.67	0.3421	2.0806	167.90

Preliminary tests of GO coatings have started through numerous brushing experiments on spare stone samples to determine the maximum concentration of GO in solution, so as brushing the stone surface two times would not alter the color observed with the naked eye. Ultimately, for a GO water dispersion, a concentration of 0.5 mg/mL was the upper limit, which we decided to use further. For two brushings, the GO quantity applied on the stone surface was calculated to be about 1.96 $\mu g/cm^2$.

Knowledge obtained from the dispersability tests was also used with the goal of obtaining the best possible dispersion of GO-OL, the improved GO fraction with excellent self-assembly capabilities. As such, a part of the existing GO water dispersion resulted from the regular synthesis pathway was further refined to obtain a GO-OL dispersion in the best solvent of choice, a mixture of water and ethanol with 60 vol.% consisting of ethanol. The newly obtained GO-OL dispersion was used for the preliminary trials, similarly to the regular GO water dispersion. Surprisingly, though, it seemed that the application of GO-OL was more difficult, as it tended to agglomerate on the lateral sides of the brushed areas, similar to a gel, which was harder to properly disperse. This was put on the behalf of the quick self-assembly of GO-OL, as well as the evaporation of ethanol in the solvent, which left a more concentrated and viscous GO-OL dispersion in water.

Furthermore, we noticed that the colour of the GO-OL coatings have darkened significantly after leaving them for one week at ambient temperature and humidity. By comparison, the coatings obtained from the regular GO water dispersions did not show any color change. Due to difficulties arising from improper application, quick evaporation, and significant color change with time, we decided to continue with coating tests obtained from the regular GO water dispersion, which is identical to the GO-init dispersion in 0% ethanol, described in Section 3.1.

Weathering of GO coatings was simulated by exposure to a UV lamp (λ = 254 nm). After some preliminary trials, a 7-hour exposure time was selected because no additional changes were noticed in the color of the coating or the XRD diffractograms of the UV-exposed GO coatings after that time.

In order to discuss their structure, we prepared GO coatings on glass slides, using the same 0.5 mg/mL GO water dispersion used for the stone brushing. FT-IR, Raman spectroscopy, and XRD analysis was performed on regular and UV-exposed coatings (Figure 3.14).

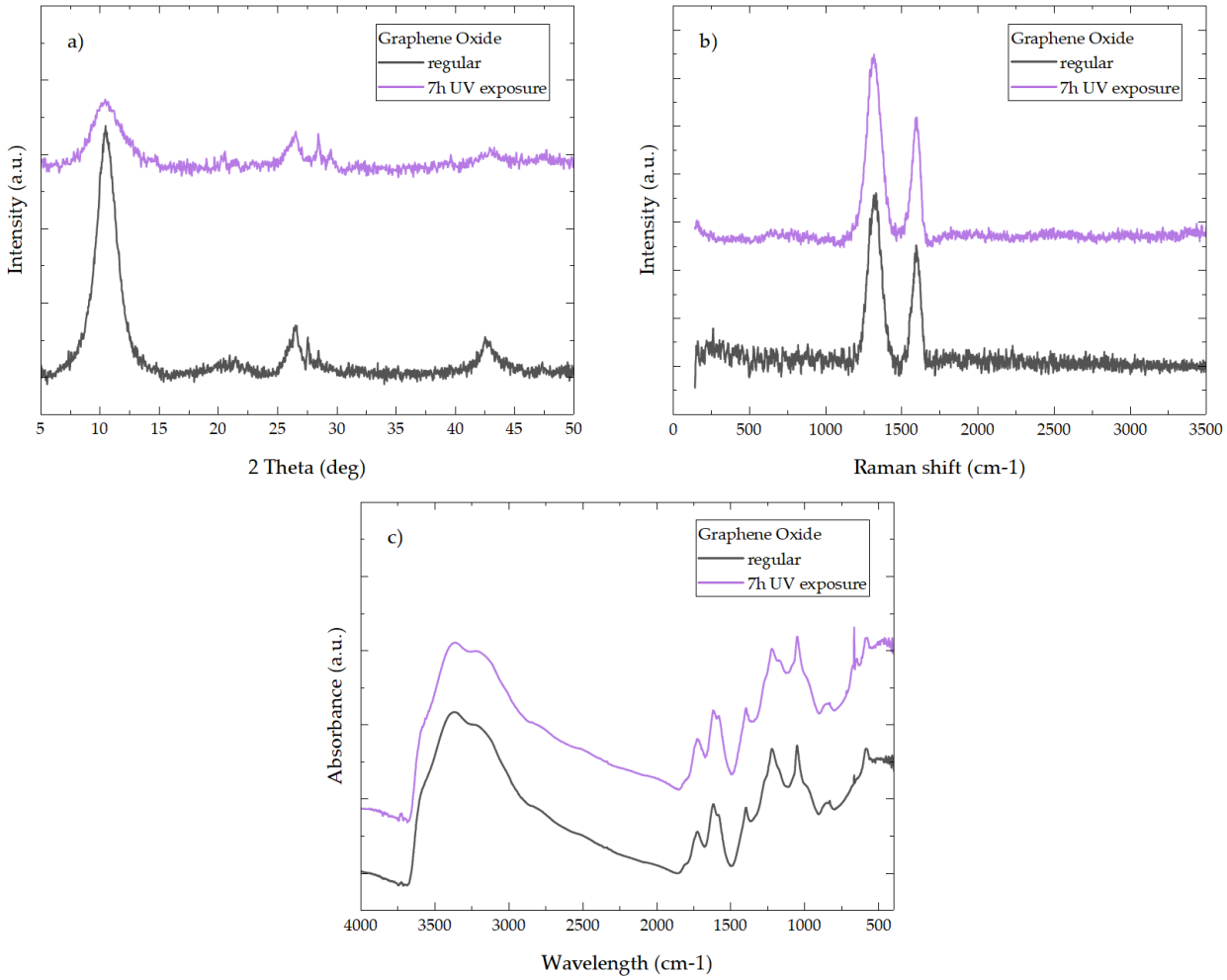

Figure 3.14: *XRD diffractograms (a), Raman spectra (785 nm excitation wavelength) (b), and transmission FT-IR spectra (KBr pellet method) (c) of GO coatings before and after their exposure for 7 hours to UV light (λ = 254 nm).*

Due to the low concentration used for preparing the films, continuous films could not form through self-assembly processes, and the coatings rather looked like dried, fragmented clusters, tightly bound to the glass substrate. No noticeable difference can be seen in the XRD patterns and the FT-IR spectra between the regular GO samples and the GO-init water dispersion (0% ethanol) discussed in Section 3.1, indicating that the structure and oxygen functional groups are still maintained in these conditions. The calculated I_D/I_G ratio were 1.47 and 1.48 for the GO and GO-UV samples. An increase compared to the 0.90 I_D/I_G ratio of the corresponding GO-init water dispersion discussed earlier can be caused by the discontinuous nature of the dried GO material. This corresponds to a larger amount of structural defects increasing I_D, due to distortions in the structure.

The UV exposure greatly changes the color of the samples, as the films become darker, which might be an indication of the expected photoreduction of the oxygen functional groups. However, no noticeable changes appear in the FT-IR or in the Raman spectra of GO samples. Still, a noticeable decrease in crystallinity is observed for the XRD diffractograms. We theorize that the UV exposure is only able to reduce the first few layers of GO, hence the color change, but in depth changes might not happen due to the low penetration depth of the UV light. More surface analysis might be needed to fully clarify this observed phenomena.

Natural and aged Euganean trachyte and Vicenza stone samples have been used for the analysis of GO coating influence on the water vapour resistance factor and the coefficient of absorption through capillarity. Three samples were used for each type of stone. First, the uncoated samples were tested, and the tests were done again after coating the same samples and later exposing them to UV light. Results are represented in Table 3.3, and a graphical version is pictured in Figure 3.15.

Table 3.3: *Mean values of water-related petrophysical properties determined on natural and aged samples of Euganean trachyte and Vicenza stone. Values in parentheses represent the percentile change against the uncoated sample.*

Sample	Coating	Water vapour resistance factor (wet-cup)	Water absorption coefficient by capillarity ($kg/m^2\ h^{1/2}$)
ET Natural	uncoated	108.81 ± 2.15	0.328 ± 0.014
	GO	124.40 ± 4.47 (14.3%)	0.253 ± 0.018 (-23.0%)
	GO-UV	114.18 ± 7.32 (4.9%)	0.167 ± 0.010 (-49.0%)
ET Aged	uncoated	110.56 ± 6.49	0.319 ± 0.016
	GO	118.31 ± 11.20 (7.0%)	0.241 ± 0.011 (-24.5%)
	GO-UV	119.68 ± 5.18 (8.2%)	0.193 ± 0.014 (-39.5%)
VS Natural	uncoated	20.73 ± 0.54	8.027 ± 0.658
	GO	24.15 ± 0.40 (16.5%)	7.186 ± 0.160 (-10.50%)
	GO-UV	21.49 ± 0.58 (3.7%)	7.073 ± 0.164 (-11.9%)
VS Aged	uncoated	20.89 ± 0.55	15.433 ± 0.508
	GO	24.66 ± 0.73 (18.0%)	13.118 ± 1.276 (-15.0%)
	GO-UV	21.39 ± 1.10 (2.4%)	11.998 ± 1.295 (-22.3%)

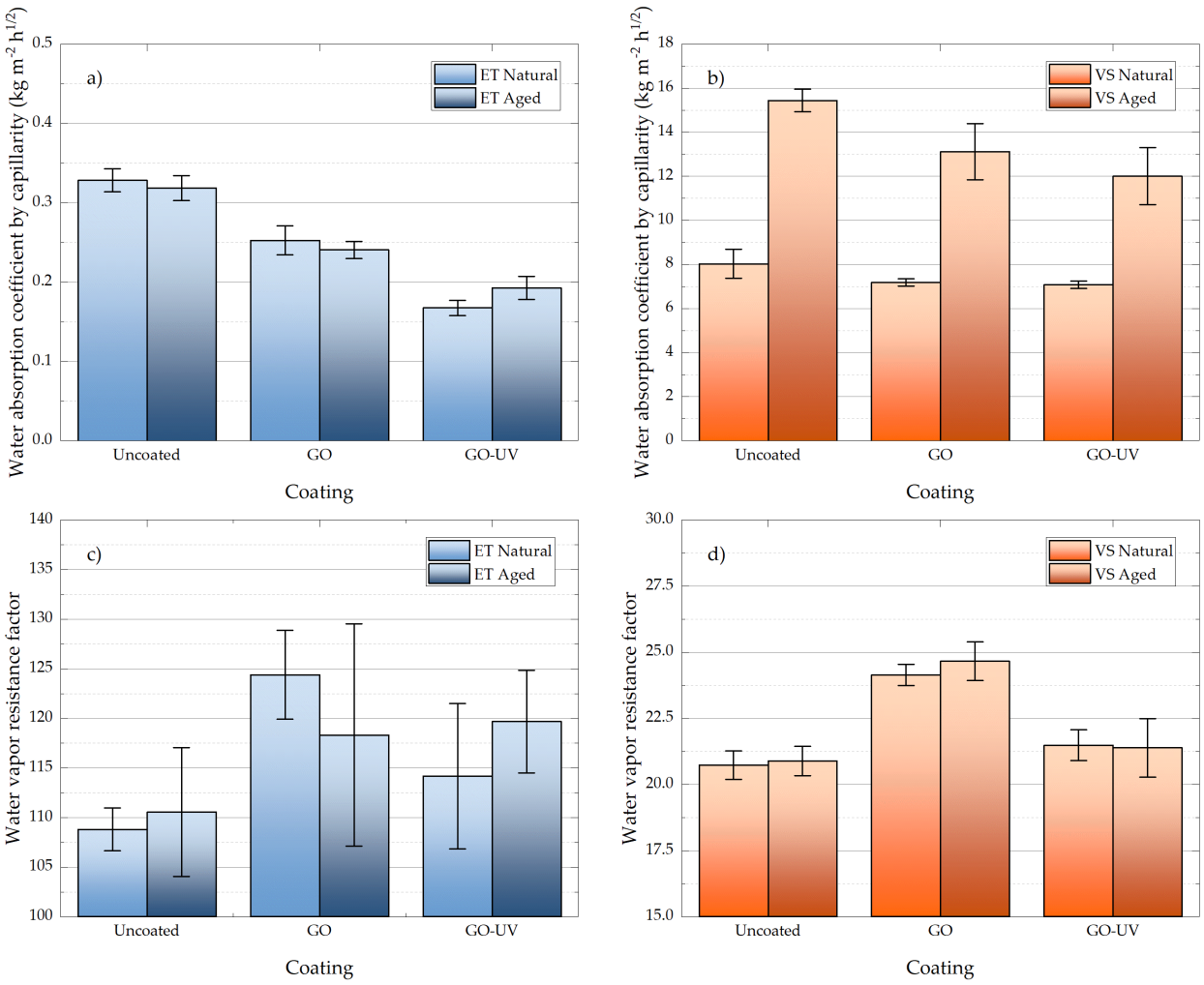

Figure 3.15: *Water absorption coefficient by capillarity and water vapor resistance factor of Euganean Trachyte (a, c) and Vicenza stone (b, d) samples.*

The artificial ageing process does not generally incur large changes to the water-related petrophysical properties of the stone samples, with the exception of the water absorption coefficient by capillary of Vicenza stone, for which large differences are noticed. This is probably a result of the pore size distribution variation after the artifical ageing, which greatly increases the open porosity for this type of stone.

A large reduction of the water capillary absorption coefficient is observed, especially for Euganean trachyte stone samples, where a decrease of up to 49.0% was reported. A lower effectiveness is seen for Vicenza stone samples, where a decrease of up to 22.3% is reported. Water capillary absorption curves can be seen in Figure 3.16. Generally, GO-UV performed better than a fresh GO coating, which might be due to the surface reduction following the UV exposure, capable of offering a degree of hydrophobicity to the GO coating.

Water vapor resistance factors of each sample suffered changes of up to 14.3 % for Euganean trachyte and 18% for Vicenza stone. In some cases, however, the change is not distinguishable from the stone sample variability. It can be noticed that GO coatings incurred the largest changes to this parameter.

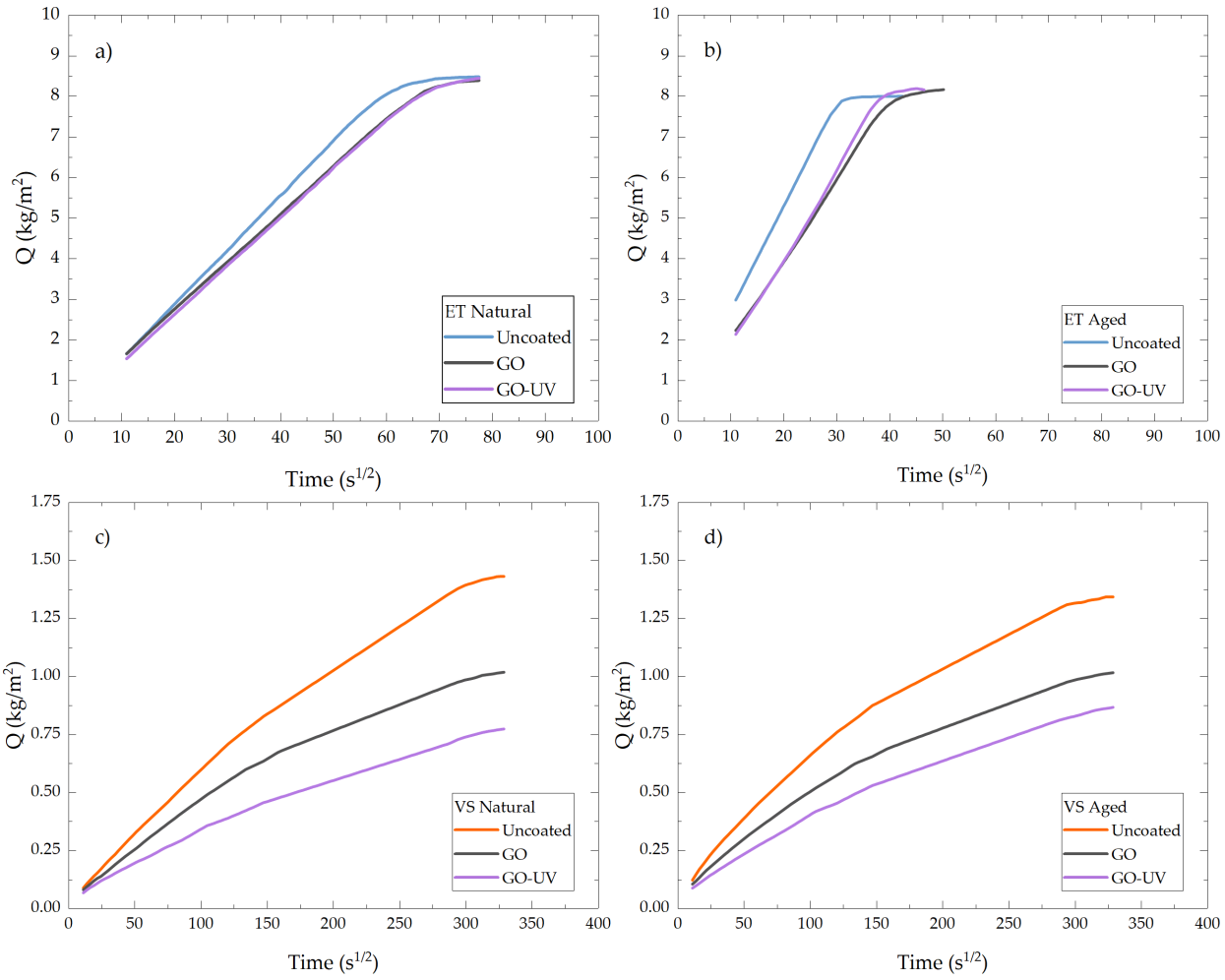

Figure 3.16: *Water capillary absorption curves of Euganean trachyte and Vicenza stone samples with their respective coatings. The average result obtained from three samples is shown.*

Similarly, water contact angle measurements were performed for each type of stone, in order to investigate the degree of hydrophilicity or hydrophobicity due to the presence of the coatings. Tests were done on three samples of natural stone, which were subsequently aged, coated with GO, and later exposed to UV light. In each case, no reliable measurement was possible for the Vicenza stone samples, due to their high water absorption, a consequence of its large open porosity. Results were only obtained for Euganean trachyte stone samples, and are represented in Figure 3.17 as the individual values for each of the three stone samples used. A large variation is naturally observed for the results obtained from the fresh stone samples, which is not observed after the ageing process takes place. Most notably, however, is that the GO coating does not change the hydrophilicity of the stone surface. A slight shift towards hydrophobicity is noticed after the UV exposure, which is a confirmation for the photoreduction of GO when subjected to UV radiation.

Colorimetric investigations were performed on the same stone samples used for the water contact angle measurements. Three measurements were done on the same five points on the surface of each sample. In accordance to Equation 2.1, color variation ΔE^* was calculated, and the results are represented in Figure 3.18.

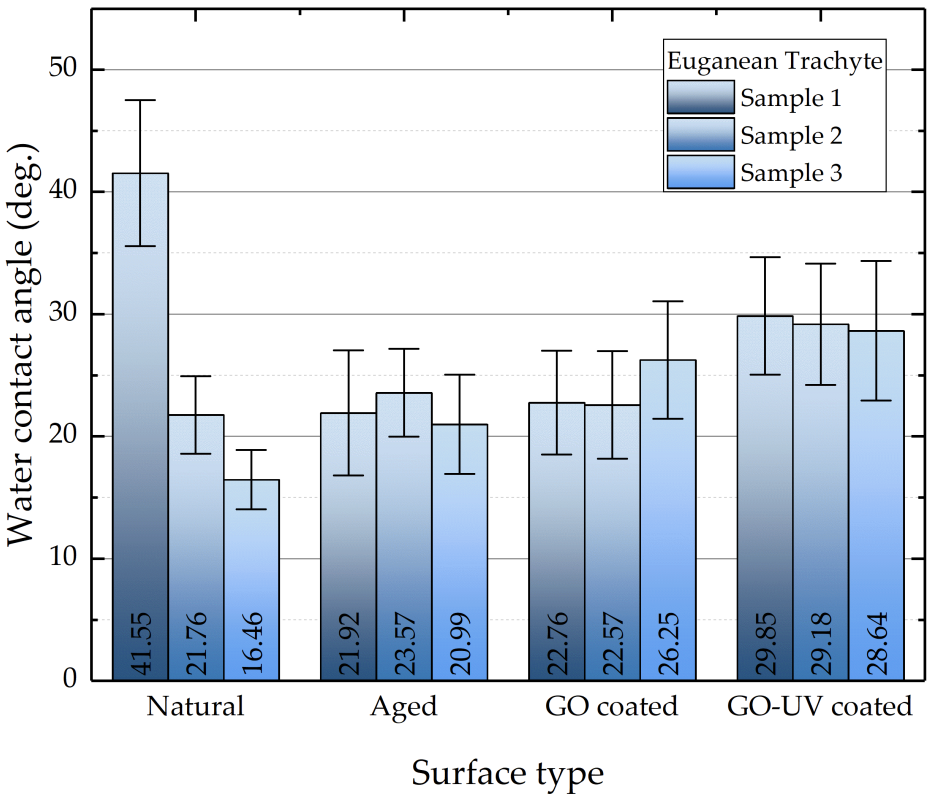

Figure 3.17: *Water contact angle measurements for three samples of Euganean trachyte. For each sample, 15 measurements were made, and the results were averaged.*

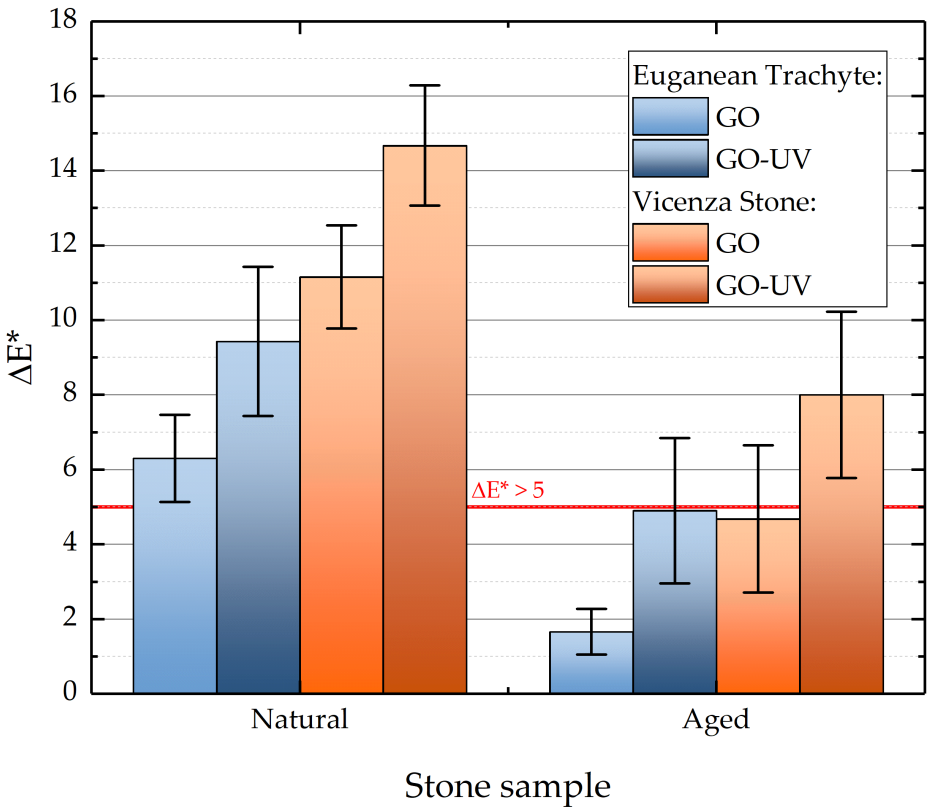

Figure 3.18: *Color variations calculated for each coating.*

Applying GO coatings on natural, fresh stone samples would lead to a color change greater than the accepted value for cultural heritage applications. Moreover, it seems that the weathering of the coating is further increasing the color difference. However, applying the GO coatings on already aged stone samples (which ideally should emulate real monuments subjected to natural weathering processes) does not produce a color change much greater than the acceptable limit. This is especially true for Euganean trachyte, which is a gray type of stone. In the case of the white Vicenza stone, GO exposure to UV radiation would lead to a much larger color difference than the acceptable range.

In order to elucidate the interaction mechanisms of GO with the stone substrate, we performed additional investigations on the morphology of the coatings. Figure 3.19 shows different features observed through optical microscopy. SEM investigations were successfully performed on Euganean trachyte samples, and are shown in Figure 3.20. SEM tests were also made on Vicenza stone samples, but due to the insulating nature of the stone, clear pictures couldn't have been taken, and we chose not to perform any surface metallization which would contaminate the thin GO coatings.

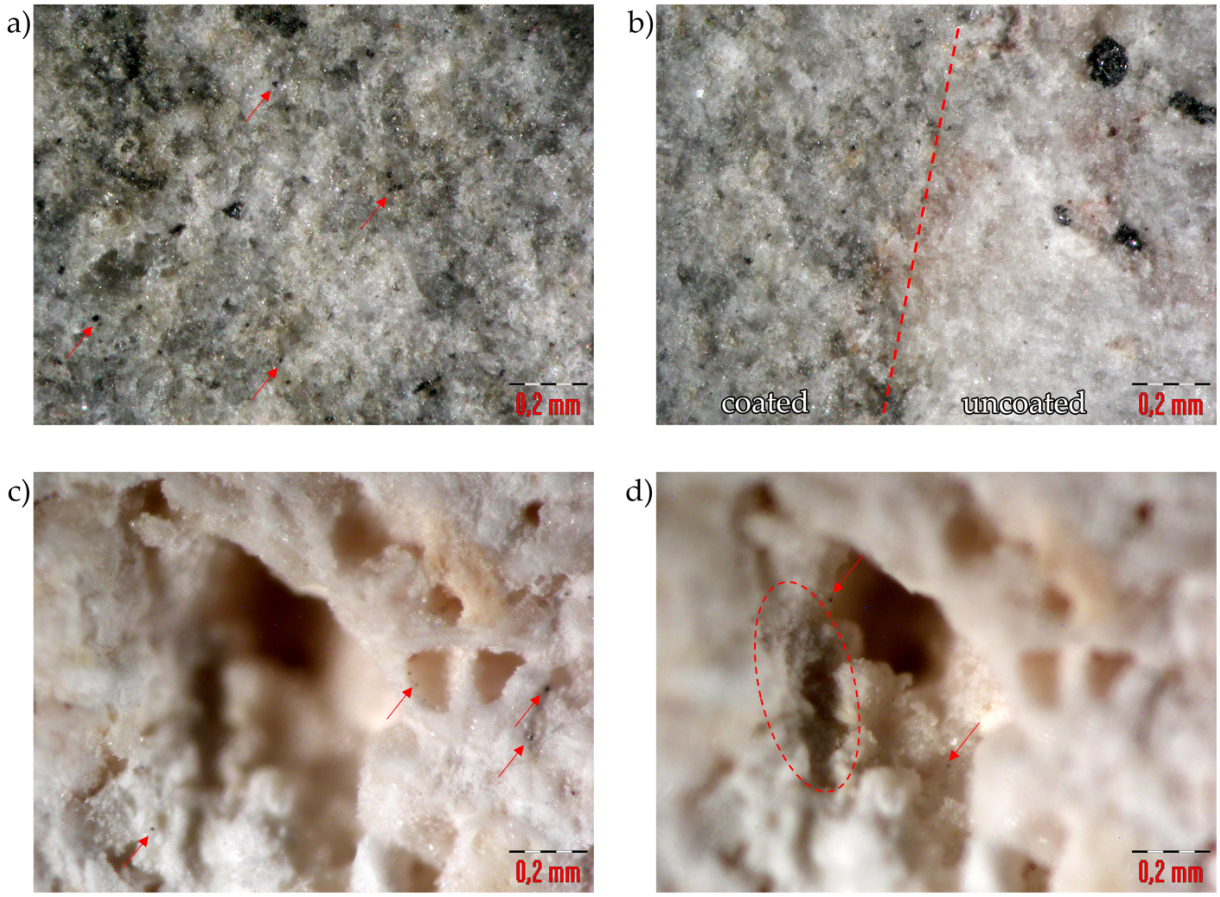

Figure 3.19: *Optical images of: a) Euganean trachyte coated with GO; b) edge of coated area on the surface of Euganean trachyte; c-d) Vicenza stone coated with GO, with a focus on the outside and inside of a pore. Red markings indicate distinctive features observed.*

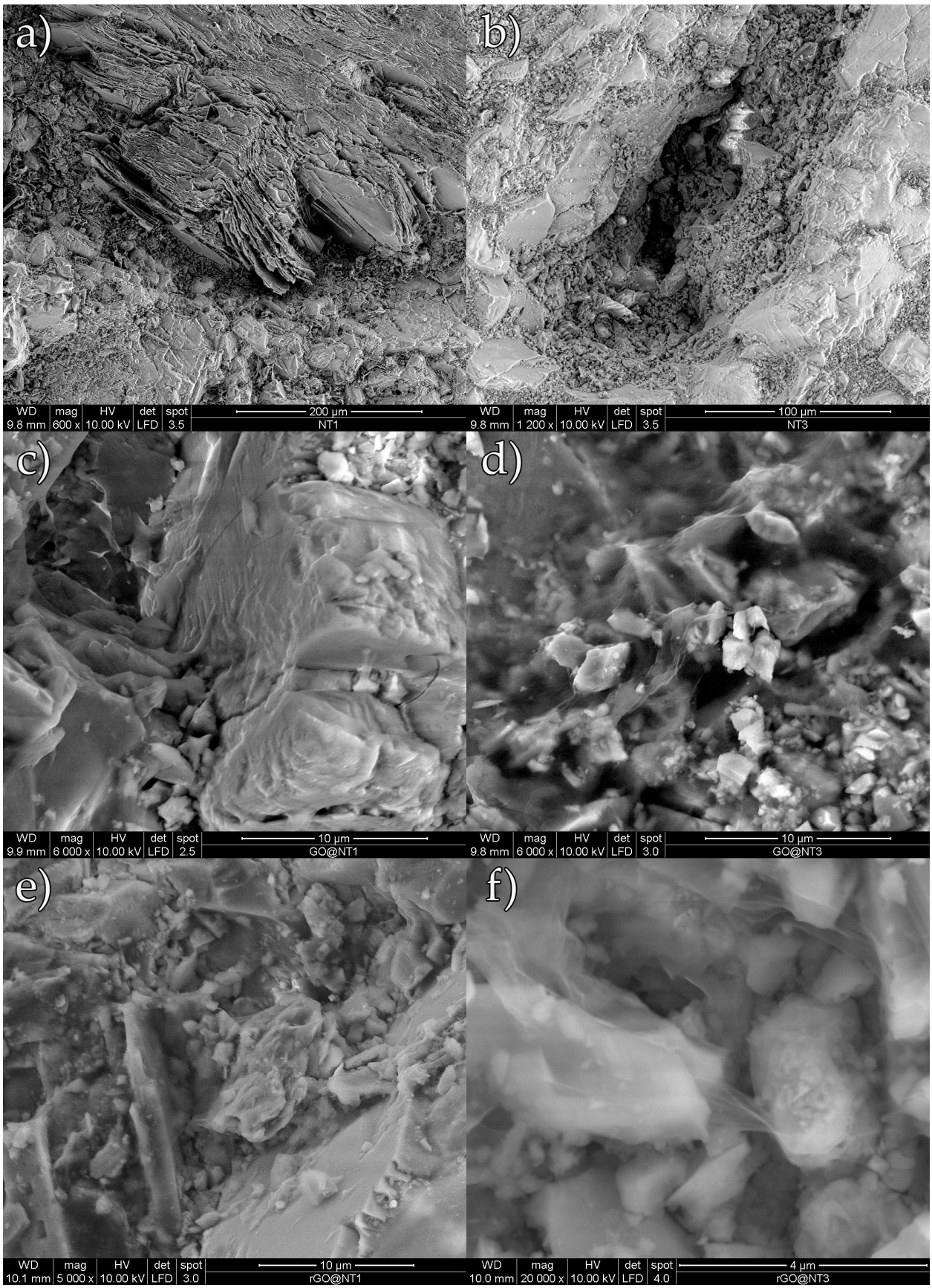

Figure 3.20: *SEM images of Euganean trachyte stone samples: a-b) uncoated; c-d) GO coated; e-f) GO-UV coated natural and aged stones, respectively. Best images have been selected from each sample type, with the goal of showing the most interesting features noticed.*

Optical microscopy shows numerous black flakes on the coated surfaces, which might consist of GO agglomerations already present in the dispersion, or formed immediately after the coating was applied. Figure 3.19b, shows a clear demarcation line between the coated and uncoated areas of the surface. Although dark flakes are noticed on the coated section, there is also a visible darkening of the surface. Figure 3.19c-d shows the image of a 1 mm wide pore on a GO coated Vicenza stone. A dark area can be identified inside the pore, where possible GO agglomeration might have happened. Generally, a relatively non-homogeneous coating is observed from the optical images, with a predisposition to GO agglomeration.

SEM images did not show any observable differences between the natural and aged stone surface, that might not be due to the natural stone variety. Similarly, no observable differences can be seen between the aspect of GO and GO-UV coatings. As such, images shown in Figure 3.20 showcase the most interesting features observed from each sample. Both GO and GO-UV have been reliably found in smaller or larger agglomerations on the surface features such as pores or edges, while on flat features of the stone it was more difficult to observe. Their aspect is similar to a thin and transparent veil, which blurs the stone features underneath, generating difficulties in properly focusing images during SEM operation. In numerous cases, it appears to bridge or cover smaller pores or spaces between stone features.

Coating morphology investigations suggest the formation of a non-uniform coating with a predisposition of agglomeration on surface features such as pores or edges. A very thin, difficult to observe coating is present on flatter surface features. Optical microscopy has also shown the presence of large flakes of agglomerated GO sheets, but it is unclear if they might originate from an improper GO dispersion or have been formed after the coating was applied. Taking this into account, we might consider two types of GO coating domains: a thick GO domain formed by agglomerated flakes in pores, and a thin GO domain found on flat surface features.

As such, we tried to obtain further information from the Raman spectra of pore and surface domains, with the aid of the Raman microscope (Figure 3.21). For Euganean trachyte samples we have observed some overlapping bands probably corresponding to organic matter contaminating the surface. In the case of Vicenza stone samples, the characteristic ν_1 symmetric stretching of CO_3 ion is observed at 1090 cm^{-1} [76]. Each spectrum was analyzed, and the I_D/I_G ratio was computed. By fitting the two D and G bands, the full width at half maximum (FWHM) of each band was recorded. The results are shown in Table 3.4.

A noticeable trend is visible when comparing the D and G band parameters of GO and GO-UV coatings between pore and surface domains for Vicenza stone. It seems that UV exposure is affecting the surface domains, more than pore domains, for which almost no change was noticed in the I_D/I_G ratio. Looking at FWHM of D and G bands of pore domains, it seems that the FWHM values of both bands are closer to the values obtained

for reference GO and GO-UV samples. Larger variations appear for surface domains, especially for the D band. Trends are harder to observe for Euganean trachyte samples, mostly due to the bands corresponding to the contamination, which overlap the D and G bands of GO.

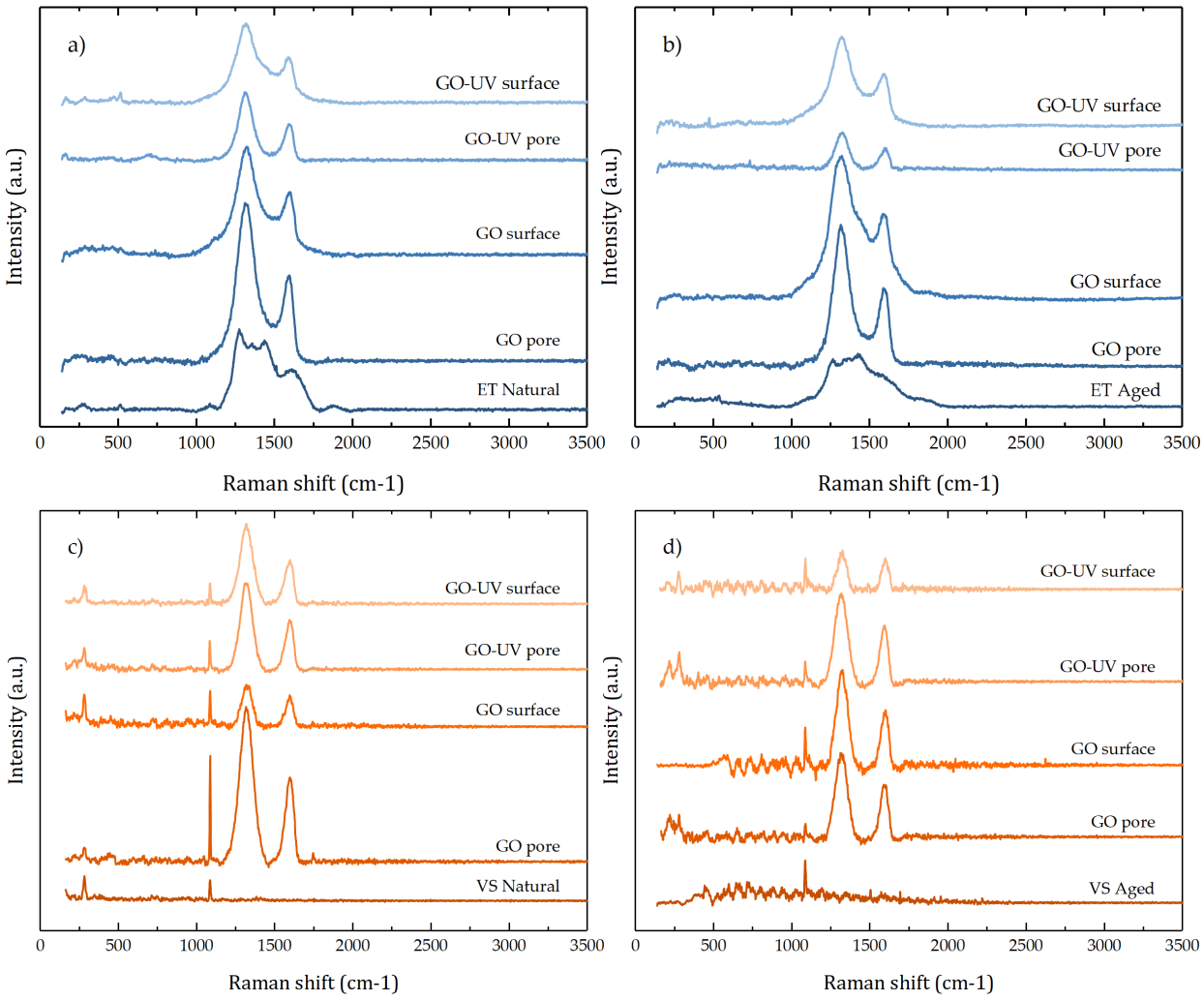

Figure 3.21: *Raman spectra of GO and GO-UV coated natural (a, c) and aged (b, d) Euganean trachyte and Vicenza stone samples, respectively. Spectra have been taken with the aid of the microscope from visible flat surfaces or pores.*

Based on this results for the Vicenza stone, we might theorize that the exposure to UV radiation is strongly affecting the thin surface domains, rather than the pore domains, where thicker GO agglomerations were noticed. By extrapolating this idea for Euganean trachyte, as well, we might be able to clarify some of the mechanisms behind the improvement of water contact angle and water capillary absorption results for GO-UV, while maintaining a relatively low modification of the water vapor resistance factor. It is known that GO has shown excellent water vapor permeation, when compared to its RGO counterpart [77, 78]. As such, there is a possibility that the pore domains of the coating are not affected by the UV radiation and maintain a free path for the permeation of water vapors inside the pores, while the surface domains suffer the chemical reduc-

tion, being responsible for the changes we noticed. Additional investigations should be performed to fully understand the unique barrier properties of GO materials, which have shown to prevent the permeation of larger ions, thus lowering the risk of salt crystallization inside the stone matrix.

Table 3.4: *Calculated D and G band parameters from the Raman spectrum of each sample.*

Sample	Coating	Surface Feature	I_D/I_G ratio	FWHM D band (cm^{-1})	FWHM G band (cm^{-1})
GO			1.47	104.32	64.79
GO-UV			1.48	113.22	63.60
ET Natural	GO	pore	1.95	163.92	110.15
		surface	1.76	195.66	135.34
	GO-UV	pore	1.82	121.13	75.93
		surface	1.89	196.43	153.41
ET Aged	GO	pore	1.87	147.70	111.47
		surface	1.93	166.37	129.22
	GO-UV	pore	1.78	103.52	70.09
		surface	1.66	214.45	122.42
VS Natural	GO	pore	1.79	105.32	63.62
		surface	1.44	77.50	57.34
	GO-UV	pore	1.78	92.87	62.09
		surface	1.80	101.22	67.14
VS Aged	GO	pore	1.56	90.88	57.36
		surface	1.72	86.00	56.62
	GO-UV	pore	1.56	94.26	57.99
		surface	1.22	66.83	51.80

Differences in FWHM of both D and G bands have been identified, which is an indicator of the formation of chemical bonds with the stone substrate. We attempted to identify the type of bond formed through ATR FT-IR investigations, but we didn't manage to obtain any signal from the GO coating, as it is consists of a very low amount of 1.96 $\mu g/cm^2$. More surface analysis should be performed to fully identify the chemical bond formed.

Recently, leachate analysis has been performed on GO stone coatings, which have shown that GO does not leach into the environment following intense water pour on coated dolomite stone surface [42]. This also hints towards the formation of a strong bond with the stone substrate, as well as eliminating the concerns of any associated health or environmental risk after the coating has been applied.

Chapter 4

Conclusions and future perspectives

The present work analysed the surface characteristics of GO synthesized through a chemical sono-exfoliation method which uses the precursors of the Marcano-Tour process. The first part of the thesis addressed the dispersability capabilities of GO in a water and ethanol solvent mixture, which led to the improvement of the refining process used to obtain the GO-OL fraction with excellent self-assembly properties. Physio-chemical analysis on liquid dispersions and self-assembled films followed, in which it was found that the GO-OL fraction lacks the leftover graphitic material from incomplete exfoliation.

On the basis of the Hansen solubility theory, we found the Hansen solubility parameters of GO-init (δ_D = 15.6 $MPa^{1/2}$; δ_P = 13.1 $MPa^{1/2}$; δ_H = 33.1 $MPa^{1/2}$) and GO-OL (δ_D = 15.7 $MPa^{1/2}$; δ_P = 11.7 $MPa^{1/2}$; δ_H = 28.6 $MPa^{1/2}$) fractions, which can be further used to find the optimum solvent for properly dispersing GO, according to the application. Results confirmed that the oxidized domains of GO dominate the dispersion mechanisms due to the presence of oxygen functional groups capable of forming hydrogen-bonds with the solvent molecules.

Then, we performed a systematic analysis on the performance of GO as a protective coating for stone cultural heritage. Tests were done on two types of stones: Euganean trachyte and Vicenza stone, which have been historically used as dimension stones for buildings or pavements in Northeast Italy. An artificial ageing process was also used for the stone samples, to simulate stone conditions of real monuments.

Preliminary trials have also been performed with GO-OL, but due to a combined effect of its quick self-assembly and faster evaporation of the ethanol in the solvent, a proper coating was difficult to obtain through brushing. We believe that this GO-OL fraction still has the potential to be used for stone coatings, but additional research is needed to identify the proper concentration and application technique to be used.

In accordance to the requirements for protective coatings in cultural heritage, GO has shown capable of maintaining a minimal change in water vapour permeability of the substrate, while reducing the water absorption coefficient by capillarity by up to 49.0% for Euganean trachyte, and 22.3% for Vicenza stone. Color changes have also been quantified, and the application of GO might seem suitable for darker stones. In the case of

Euganean trachyte, average color changes do not surpass the $\Delta E^* < 5$ limit, while for the Vicenza stone the changes are larger than accepted. The durability of the GO coating might be estimated by the UV induced changes on its characteristics, which improved its performance, at the cost of darkening its color. Using a less concentrated GO dispersion might also mitigate the aesthetic variations, at the cost of reducing the performance. Better results have been obtained for the Euganean trachyte than the Vicenza stone, which might be due to its lower open porosity and pore size.

Overall, GO has shown promising results towards the possibility of being used as a protective stone coating. Further tests should consist in the identification of the chemical bonds formed with the stone substrate, as well as its selective barrier properties which might prevent the access of air pollutants inside the stone matrix, thus preventing potential salt crystallization. Investigating the well-known antimicrobial capabilities of GO in stopping algae and fungi formation on exposed stone surfaces would complete the full picture of the protective efficacy of GO against the most common stone weathering mechanisms. Different application methods such as spray-coating should also be tested, as well as performing additional trials with the GO-OL fraction. Besides this, it would be worth trying to functionalize GO with components such as TiO_2, which might help in mitigating the darkening effect of GO.

References

[1] M. Steiger, A. E. Charola, and K. Sterflinger, "Weathering and Deterioration," in *Stone in Architecture: Properties, Durability*, S. Siegesmund and R. Snethlage, Eds. Berlin, Heidelberg: Springer, 2014, pp. 225–316. [Online]. Available: https://doi.org/10.1007/978-3-642-45155-3_4

[2] S. Basu, S. A. Orr, and Y. D. Aktas, "A Geological Perspective on Climate Change and Building Stone Deterioration in London: Implications for Urban Stone-Built Heritage Research and Management," *Atmosphere*, vol. 11, no. 8, p. 788, Aug. 2020. [Online]. Available: https://www.mdpi.com/2073-4433/11/8/788

[3] S. Siegesmund and R. Snethlage, Eds., *Stone in Architecture: Properties, Durability*. Berlin, Heidelberg: Springer, 2014. [Online]. Available: https://link.springer.com/10.1007/978-3-642-45155-3

[4] S. Fatorić and E. Seekamp, "Are cultural heritage and resources threatened by climate change? A systematic literature review," *Climatic Change*, vol. 142, no. 1, pp. 227–254, May 2017. [Online]. Available: https://doi.org/10.1007/s10584-017-1929-9

[5] E. Sesana, A. S. Gagnon, C. Ciantelli, J. Cassar, and J. J. Hughes, "Climate change impacts on cultural heritage: A literature review," *WIREs Climate Change*, vol. 12, no. 4, p. e710, 2021. [Online]. Available: https://onlinelibrary.wiley.com/doi/abs/10.1002/wcc.710

[6] F. Gherardi, "Current and Future Trends in Protective Treatments for Stone Heritage," in *Conserving Stone Heritage: Traditional and Innovative Materials and Techniques*, ser. Cultural Heritage Science, F. Gherardi and P. N. Maravelaki, Eds. Cham: Springer International Publishing, 2022, pp. 137–176. [Online]. Available: https://doi.org/10.1007/978-3-030-82942-1_5

[7] F. Gherardi and P. N. Maravelaki, Eds., *Conserving Stone Heritage: Traditional and Innovative Materials and Techniques*, ser. Cultural Heritage Science. Cham: Springer International Publishing, 2022. [Online]. Available: https://link.springer.com/10.1007/978-3-030-82942-1

[8] A. E. Charola, "Water-Repellent Treatments for Building Stones: A Practical Overview," *APT Bulletin: The Journal of Preservation Technology*, vol. 26, no. 2/3, pp. 10–17, 1995. [Online]. Available: https://www.jstor.org/stable/1504480

[9] R. Snethlage, "Stone Conservation," in *Stone in Architecture: Properties, Durability*, S. Siegesmund and R. Snethlage, Eds. Berlin, Heidelberg: Springer, 2014, pp. 415–550. [Online]. Available: https://doi.org/10.1007/978-3-642-45155-3_7

[10] A. Sierra-Fernandez, L. S. Gomez-Villalba, M. E. Rabanal, and R. Fort, "New nanomaterials for applications in conservation and restoration of stony materials: A review," *Materiales de Construcción*, vol. 67, no. 325, pp. e107–e107, Mar. 2017. [Online]. Available: https://materconstrucc.revistas.csic.es/index.php/materconstrucc/article/view/2161

[11] I. Karapanagiotis and M. Hosseini, "Superhydrophobic Coatings for the Protection of Natural Stone," in *Advanced Materials for the Conservation of Stone*, M. Hosseini and I. Karapanagiotis, Eds. Cham: Springer International Publishing, 2018, pp. 1–25. [Online]. Available: https://doi.org/10.1007/978-3-319-72260-3_1

[12] M. E. David, R.-M. Ion, R. M. Grigorescu, L. Iancu, and E. R. Andrei, "Nanomaterials Used in Conservation and Restoration of Cultural Heritage: An Up-to-Date Overview," *Materials*, vol. 13, no. 9, p. 2064, Jan. 2020. [Online]. Available: https://www.mdpi.com/1996-1944/13/9/2064

[13] V. Daniele, G. Taglieri, and R. Quaresima, "The nanolimes in Cultural Heritage conservation: Characterisation and analysis of the carbonatation process," *Journal of Cultural Heritage*, vol. 9, no. 3, pp. 294–301, Jul. 2008. [Online]. Available: https://www.sciencedirect.com/science/article/pii/S1296207408000538

[14] L. Toniolo and F. Gherardi, "The Protection of Marble Surfaces: The Challenge to Develop Suitable Nanostructured Treatments," in *Advanced Materials for the Conservation of Stone*, M. Hosseini and I. Karapanagiotis, Eds. Cham: Springer International Publishing, 2018, pp. 57–78. [Online]. Available: https://doi.org/10.1007/978-3-319-72260-3_3

[15] I. Franco-Castillo, L. Hierro, J. M. de la Fuente, A. Seral-Ascaso, and S. G. Mitchell, "Perspectives for antimicrobial nanomaterials in cultural heritage conservation," *Chem*, vol. 7, no. 3, pp. 629–669, Mar. 2021. [Online]. Available: https://www.sciencedirect.com/science/article/pii/S2451929421000358

[16] A. M. Ferrari, M. Pini, P. Neri, and F. Bondioli, "Nano-TiO2 Coatings for Limestone: Which Sustainability for Cultural Heritage?" *Coatings*, vol. 5, no. 3, pp. 232–245, Sep. 2015. [Online]. Available: https://www.mdpi.com/2079-6412/5/3/232

[17] L. S. Gomez-Villalba, C. Salcines, and R. Fort, "Application of Inorganic Nanomaterials in Cultural Heritage Conservation, Risk of Toxicity, and Preventive Measures," *Nanomaterials*, vol. 13, no. 9, p. 1454, Jan. 2023. [Online]. Available: https://www.mdpi.com/2079-4991/13/9/1454

[18] J. M. D. Calmeiro, J. P. C. Tomé, and L. M. O. Lourenço, "Supramolecular graphene–phthalocyanine assemblies for technological breakthroughs," *Journal of Materials Chemistry C*, vol. 8, no. 25, pp. 8344–8361, Jul. 2020. [Online]. Available: https://pubs.rsc.org/en/content/articlelanding/2020/tc/d0tc00557f

[19] O. C. Compton and S. T. Nguyen, "Graphene Oxide, Highly Reduced Graphene Oxide, and Graphene: Versatile Building Blocks for Carbon-Based Materials," *Small*, vol. 6, no. 6, pp. 711–723, 2010. [Online]. Available: https://onlinelibrary.wiley.com/doi/abs/10.1002/smll.200901934

[20] C. Chung, Y.-K. Kim, D. Shin, S.-R. Ryoo, B. H. Hong, and D.-H. Min, "Biomedical Applications of Graphene and Graphene Oxide," *Accounts of Chemical Research*, vol. 46, no. 10, pp. 2211–2224, Oct. 2013. [Online]. Available: https://doi.org/10.1021/ar300159f

[21] S. Korkmaz and İ. A. Kariper, "Graphene and graphene oxide based aerogels: Synthesis, characteristics and supercapacitor applications," *Journal of Energy Storage*, vol. 27, p. 101038, Feb. 2020. [Online]. Available: https://www.sciencedirect.com/science/article/pii/S2352152X19310795

[22] W. S. J. Hummers and R. E. Offeman, "Preparation of Graphitic Oxide," *Journal of the American Chemical Society*, vol. 80, no. 6, pp. 1339–1339, Mar. 1958. [Online]. Available: https://doi.org/10.1021/ja01539a017

[23] J. Chen, B. Yao, C. Li, and G. Shi, "An improved Hummers method for eco-friendly synthesis of graphene oxide," *Carbon*, vol. 64, pp. 225–229, Nov. 2013. [Online]. Available: https://www.sciencedirect.com/science/article/pii/S0008622313006891

[24] D. C. Marcano, D. V. Kosynkin, J. M. Berlin, A. Sinitskii, Z. Sun, A. Slesarev, L. B. Alemany, W. Lu, and J. M. Tour, "Improved Synthesis of Graphene Oxide," *ACS Nano*, vol. 4, no. 8, pp. 4806–4814, Aug. 2010. [Online]. Available: https://doi.org/10.1021/nn1006368

[25] R. Tarcan, O. Todor-Boer, I. Petrovai, C. Leordean, S. Astilean, and I. Botiz, "Reduced graphene oxide today," *Journal of Materials Chemistry C*, vol. 8, no. 4, pp. 1198–1224, 2020. [Online]. Available: https://pubs.rsc.org/en/content/articlelanding/2020/tc/c9tc04916a

[26] J.-J. Shao, W. Lv, and Q.-H. Yang, "Self-Assembly of Graphene Oxide at Interfaces," *Advanced Materials*, vol. 26, no. 32, pp. 5586–5612, 2014. [Online]. Available: https://onlinelibrary.wiley.com/doi/abs/10.1002/adma.201400267

[27] L. C. Cotet, K. Magyari, M. Todea, M. C. Dudescu, V. Danciu, and L. Baia, "Versatile self-assembled graphene oxide membranes obtained under ambient conditions by using a water–ethanol suspension," *Journal of Materials Chemistry A*, vol. 5, no. 5, pp. 2132–2142, Jan. 2017. [Online]. Available: https://pubs.rsc.org/en/content/articlelanding/2017/ta/c6ta08898h

[28] R. Alrammouz, J. Podlecki, A. Vena, R. Garcia, P. Abboud, R. Habchi, and B. Sorli, "Highly porous and flexible capacitive humidity sensor based on self-assembled graphene oxide sheets on a paper substrate," *Sensors and Actuators B: Chemical*, vol. 298, p. 126892, Nov. 2019. [Online]. Available: https://www.sciencedirect.com/science/article/pii/S0925400519310913

[29] F. Zhong, Y. He, P. Wang, C. Chen, Y. Lin, Y. Wu, and J. Chen, "Self-assembled graphene oxide-graphene hybrids for enhancing the corrosion resistance of waterborne epoxy coating," *Applied Surface Science*, vol. 488, pp. 801–812, Sep. 2019. [Online]. Available: https://www.sciencedirect.com/science/article/pii/S0169433219316411

[30] A. Chuquitarqui, L. C. Cotet, M. Baia, E. György, K. Magyari, L. Barbu-Tudoran, L. Baia, M. Díaz-González, C. Fernández-Sánchez, and A. P. D. Pino, "New fabrication method for producing reduced graphene oxide flexible electrodes by using a low-power visible laser diode engraving system," *Nanotechnology*, vol. 31, no. 32, p. 325402, May 2020. [Online]. Available: https://dx.doi.org/10.1088/1361-6528/ab8d67

[31] W. Wu, Y. Shi, G. Liu, X. Fan, and Y. Yu, "Recent development of graphene oxide based forward osmosis membrane for water treatment: A critical review," *Desalination*, vol. 491, p. 114452, Oct. 2020. [Online]. Available: https://www.sciencedirect.com/science/article/pii/S0011916419320417

[32] R. Ding, W. Li, X. Wang, T. Gui, B. Li, P. Han, H. Tian, A. Liu, X. Wang, X. Liu, X. Gao, W. Wang, and L. Song, "A brief review of corrosion protective films and coatings based on graphene and graphene oxide," *Journal of Alloys and Compounds*, vol. 764, pp. 1039–1055, Oct. 2018. [Online]. Available: https://www.sciencedirect.com/science/article/pii/S0925838818322540

[33] D. S. Chauhan, M. A. Quraishi, K. R. Ansari, and T. A. Saleh, "Graphene and graphene oxide as new class of materials for corrosion control and protection: Present status and future scenario," *Progress in Organic Coatings*, vol. 147, p. 105741,

Oct. 2020. [Online]. Available: https://www.sciencedirect.com/science/article/pii/S0300944020300734

[34] S. S. A. Kumar, S. Bashir, K. Ramesh, and S. Ramesh, "New perspectives on Graphene/Graphene oxide based polymer nanocomposites for corrosion applications: The relevance of the Graphene/Polymer barrier coatings," *Progress in Organic Coatings*, vol. 154, p. 106215, May 2021. [Online]. Available: https://www.sciencedirect.com/science/article/pii/S0300944021000862

[35] A. Krishnamurthy, V. Gadhamshetty, R. Mukherjee, B. Natarajan, O. Eksik, S. Ali Shojaee, D. A. Lucca, W. Ren, H.-M. Cheng, and N. Koratkar, "Superiority of Graphene over Polymer Coatings for Prevention of Microbially Induced Corrosion," *Scientific Reports*, vol. 5, p. 13858, Sep. 2015.

[36] S. Liu, T. H. Zeng, M. Hofmann, E. Burcombe, J. Wei, R. Jiang, J. Kong, and Y. Chen, "Antibacterial Activity of Graphite, Graphite Oxide, Graphene Oxide, and Reduced Graphene Oxide: Membrane and Oxidative Stress," *ACS Nano*, vol. 5, no. 9, pp. 6971–6980, Sep. 2011. [Online]. Available: https://doi.org/10.1021/nn202451x

[37] S. Gurunathan, J. W. Han, A. A. Dayem, V. Eppakayala, and J.-H. Kim, "Oxidative stress-mediated antibacterial activity of graphene oxide and reduced graphene oxide in Pseudomonas aeruginosa," *International Journal of Nanomedicine*, vol. 7, pp. 5901–5914, Dec. 2012. [Online]. Available: https://www.tandfonline.com/doi/abs/10.2147/IJN.S37397

[38] S. S. Nanda, D. K. Yi, and K. Kim, "Study of antibacterial mechanism of graphene oxide using Raman spectroscopy," *Scientific Reports*, vol. 6, no. 1, p. 28443, Jun. 2016. [Online]. Available: https://www.nature.com/articles/srep28443

[39] M.-H. Wang, Q. Li, X. Li, Y. Liu, and L.-Z. Fan, "Effect of oxygen-containing functional groups in epoxy/reduced graphene oxide composite coatings on corrosion protection and antimicrobial properties," *Applied Surface Science*, vol. 448, pp. 351–361, Aug. 2018. [Online]. Available: https://www.sciencedirect.com/science/article/pii/S0169433218311012

[40] T. Arun, D. K. Ray, V. P. Gupta, S. S. Panda, P. K. Sahoo, J. Ghosh, P. Sengupta, and P. V. Satyam, "Surface protection coating material for controlling the decay of major construction stone," *AIP Conference Proceedings*, vol. 1832, no. 1, p. 080017, May 2017. [Online]. Available: https://doi.org/10.1063/1.4980477

[41] D. González-Campelo, M. Fernández-Raga, Á. Gómez-Gutiérrez, M. I. Guerra-Romero, and J. M. González-Domínguez, "Extraordinary Protective Efficacy of Graphene Oxide over the Stone-Based Cultural Heritage," *Advanced Materials Interfaces*, vol. 8, no. 23, p. 2101012, 2021. [Online]. Available: https://onlinelibrary.wiley.com/doi/abs/10.1002/admi.202101012

[42] R. Martínez-García, D. González-Campelo, F. J. Fraile-Fernández, A. M. Castañón, P. Caldevilla, S. Giganto, A. Ortiz-Marqués, F. Zelli, V. Calvo, J. M. González-Domínguez, and M. Fernández-Raga, "Performance Study of Graphene Oxide as an Antierosion Coating for Ornamental and Heritage Dolostone," *Advanced Materials Technologies*, 2023. [Online]. Available: https://onlinelibrary.wiley.com/doi/abs/10.1002/admt.202300486

[43] A. B. Seabra, A. J. Paula, R. de Lima, O. L. Alves, and N. Durán, "Nanotoxicity of Graphene and Graphene Oxide," *Chemical Research in Toxicology*, vol. 27, no. 2, pp. 159–168, Feb. 2014. [Online]. Available: https://doi.org/10.1021/tx400385x

[44] P.-P. Jia, T. Sun, M. Junaid, L. Yang, Y.-B. Ma, Z.-S. Cui, D.-P. Wei, H.-F. Shi, and D.-S. Pei, "Nanotoxicity of different sizes of graphene (G) and graphene oxide (GO) in vitro and in vivo," *Environmental Pollution*, vol. 247, pp. 595–606, Apr. 2019. [Online]. Available: https://www.sciencedirect.com/science/article/pii/S0269749118349133

[45] X. Hu, Y. Gao, and Z. Fang, "Integrating metabolic analysis with biological endpoints provides insight into nanotoxicological mechanisms of graphene oxide: From effect onset to cessation," *Carbon*, vol. 109, pp. 65–73, Nov. 2016. [Online]. Available: https://www.sciencedirect.com/science/article/pii/S0008622316306418

[46] M. C. P. Mendonça, E. S. Soares, M. B. de Jesus, H. J. Ceragioli, S. P. Irazusta, Â. G. Batista, M. A. R. Vinolo, M. R. Maróstica Júnior, and M. A. da Cruz-Höfling, "Reduced graphene oxide: Nanotoxicological profile in rats," *Journal of Nanobiotechnology*, vol. 14, no. 1, p. 53, Jun. 2016. [Online]. Available: https://doi.org/10.1186/s12951-016-0206-9

[47] Y. Zhao, Y. Liu, X. Zhang, and W. Liao, "Environmental transformation of graphene oxide in the aquatic environment," *Chemosphere*, vol. 262, p. 127885, Jan. 2021. [Online]. Available: https://www.sciencedirect.com/science/article/pii/S0045653520320804

[48] L. Serrano-Luján, S. Víctor-Román, C. Toledo, O. Sanahuja-Parejo, A. E. Mansour, J. Abad, A. Amassian, A. M. Benito, W. K. Maser, and A. Urbina, "Environmental impact of the production of graphene oxide and reduced graphene oxide," *SN Applied Sciences*, vol. 1, no. 2, p. 179, Jan. 2019. [Online]. Available: https://doi.org/10.1007/s42452-019-0193-1

[49] E. Franzoni, E. Sassoni, G. W. Scherer, and S. Naidu, "Artificial weathering of stone by heating," *Journal of Cultural Heritage*, vol. 14, no. 3, Supplement, pp. e85–e93, Jun. 2013. [Online]. Available: https://www.sciencedirect.com/science/article/pii/S1296207413000447

[50] M. Ayán-Varela, J. I. Paredes, S. Villar-Rodil, R. Rozada, A. Martínez-Alonso, and J. M. D. Tascón, "A quantitative analysis of the dispersion behavior of reduced graphene oxide in solvents," *Carbon*, vol. 75, pp. 390–400, Aug. 2014. [Online]. Available: https://www.sciencedirect.com/science/article/pii/S0008622314003376

[51] C. M. Hansen, *Hansen Solubility Parameters: A User's Handbook, Second Edition*, 2nd ed. Boca Raton: CRC Press, Jun. 2007.

[52] S. Siegesmund and Á. Török, "Building Stones," in *Stone in Architecture: Properties, Durability*, S. Siegesmund and R. Snethlage, Eds. Berlin, Heidelberg: Springer, 2014, pp. 11–95. [Online]. Available: https://doi.org/10.1007/978-3-642-45155-3_2

[53] S. Salvini, C. Coletti, L. Maritan, M. Massironi, A. Pieropan, R. Spiess, and C. Mazzoli, "Petrographic characterization and durability of carbonate stones used in UNESCO World Heritage Sites in northeastern Italy," *Environmental Earth Sciences*, vol. 82, no. 1, p. 49, Jan. 2023. [Online]. Available: https://doi.org/10.1007/s12665-022-10732-y

[54] M. Mattioli, M. Cenni, and E. Passaglia, "Secondary mineral assemblage as indicator of multistage alteration processes in basaltic lava flows: Evidence from the Lessini Mountains, Veneto Volcanic Province, Northern Italy," *Periodico di Mineralogia*, vol. 85, no. 1, 2016. [Online]. Available: https://rosa.uniroma1.it/rosa04/periodico_di_mineralogia/article/view/15874

[55] S. Scrivano, L. Gaggero, and J. Gisbert Aguilar, "An Experimental Investigation of the Effects of Grain Size and Pore Network on the Durability of Vicenza Stone," *Rock Mechanics and Rock Engineering*, vol. 52, no. 9, pp. 2935–2948, Sep. 2019. [Online]. Available: https://doi.org/10.1007/s00603-019-01768-x

[56] C. Di Benedetto, P. Cappelletti, M. Favaro, S. F. Graziano, A. Langella, D. Calcaterra, and A. Colella, "Porosity as key factor in the durability of two historical building stones: Neapolitan Yellow Tuff and Vicenza Stone," *Engineering Geology*, vol. 193, pp. 310–319, Jul. 2015. [Online]. Available: https://www.sciencedirect.com/science/article/pii/S001379521500160X

[57] L. Germinario, S. Siegesmund, L. Maritan, and C. Mazzoli, "Petrophysical and mechanical properties of Euganean trachyte and implications for dimension stone decay and durability performance," *Environmental Earth Sciences*, vol. 76, no. 21, p. 739, Oct. 2017. [Online]. Available: https://doi.org/10.1007/s12665-017-7034-6

[58] L. Germinario, J. M. Hanchar, R. Sassi, L. Maritan, R. Cossio, A. Borghi, and C. Mazzoli, "New petrographic and geochemical tracers for recognizing the provenance quarry of trachyte of the Euganean Hills, northeastern Italy," *Geoarchaeology*, vol. 33, no. 4, pp. 430–452, 2018. [Online]. Available: https://onlinelibrary.wiley.com/doi/abs/10.1002/gea.21666

[59] S. Siegesmund and H. Dürrast, "Physical and Mechanical Properties of Rocks," in *Stone in Architecture: Properties, Durability*, S. Siegesmund and R. Snethlage, Eds. Berlin, Heidelberg: Springer, 2014, pp. 97–224. [Online]. Available: https://doi.org/10.1007/978-3-642-45155-3_3

[60] B. Graue, S. Siegesmund, P. Oyhantcabal, R. Naumann, T. Licha, and K. Simon, "The effect of air pollution on stone decay: The decay of the Drachenfels trachyte in industrial, urban, and rural environments—a case study of the Cologne, Altenberg and Xanten cathedrals," *Environmental Earth Sciences*, vol. 69, no. 4, pp. 1095–1124, Jun. 2013. [Online]. Available: https://doi.org/10.1007/s12665-012-2161-6

[61] C. Costinas, C. A. Salagean, L. C. Cotet, M. Baia, M. Todea, K. Magyari, and L. Baia, "Insights into the Stability of Graphene Oxide Aqueous Dispersions," *Nanomaterials*, vol. 12, no. 24, p. 4489, Jan. 2022. [Online]. Available: https://www.mdpi.com/2079-4991/12/24/4489

[62] Standard, "EN 15803:2009 - Conservation of Cultural Property - Test methods - Determination of water vapour permeability (Δp)," 2009.

[63] ——, "EN 15801:2009 - Conservation of cultural property - Test methods - Determination of capillarity water absorption," 2009.

[64] ——, "EN 15802:2010 - Conservation of cultural property - Test methods - Determination of static contact angle," 2009.

[65] E. Zendri, L. Falchi, F. C. Izzo, Z. M. Morabito, and G. Driussi, "A review of common NDTs in the monitoring and preservation of historical architectural surfaces," *International Journal of Architectural Heritage*, vol. 11, no. 7, pp. 987–1004, Oct. 2017. [Online]. Available: https://doi.org/10.1080/15583058.2017.1331477

[66] K. Krishnamoorthy, M. Veerapandian, K. Yun, and S. J. Kim, "The chemical and structural analysis of graphene oxide with different degrees of oxidation," *Carbon*, vol. 53, pp. 38–49, Mar. 2013. [Online]. Available: https://www.sciencedirect.com/science/article/pii/S0008622312008263

[67] E. Fuente, J. A. Menéndez, M. A. Díez, D. Suárez, and M. A. Montes-Morán, "Infrared Spectroscopy of Carbon Materials: A Quantum Chemical Study of Model Compounds," *The Journal of Physical Chemistry B*, vol. 107, no. 26, pp. 6350–6359, Jul. 2003. [Online]. Available: https://doi.org/10.1021/jp027482g

[68] D. R. Dreyer, S. Park, C. W. Bielawski, and R. S. Ruoff, "The chemistry of graphene oxide," *Chemical Society Reviews*, vol. 39, no. 1, pp. 228–240, Dec. 2009. [Online]. Available: https://pubs.rsc.org/en/content/articlelanding/2010/cs/b917103g

[69] A. Dimiev, D. V. Kosynkin, L. B. Alemany, P. Chaguine, and J. M. Tour, "Pristine Graphite Oxide," *Journal of the American Chemical Society*, vol. 134, no. 5, pp. 2815–2822, Feb. 2012. [Online]. Available: https://doi.org/10.1021/ja211531y

[70] L. G. Cançado, A. Jorio, E. H. M. Ferreira, F. Stavale, C. A. Achete, R. B. Capaz, M. V. O. Moutinho, A. Lombardo, T. S. Kulmala, and A. C. Ferrari, "Quantifying Defects in Graphene via Raman Spectroscopy at Different Excitation Energies," *Nano Letters*, vol. 11, no. 8, pp. 3190–3196, Aug. 2011. [Online]. Available: https://doi.org/10.1021/nl201432g

[71] T. Zhang, G.-Y. Zhu, C.-H. Yu, Y. Xie, M.-Y. Xia, B.-Y. Lu, X. Fei, and Q. Peng, "The UV absorption of graphene oxide is size-dependent: Possible calibration pitfalls," *Microchimica Acta*, vol. 186, no. 3, p. 207, Feb. 2019. [Online]. Available: https://doi.org/10.1007/s00604-019-3329-5

[72] D. Konios, M. M. Stylianakis, E. Stratakis, and E. Kymakis, "Dispersion behaviour of graphene oxide and reduced graphene oxide," *Journal of Colloid and Interface Science*, vol. 430, pp. 108–112, Sep. 2014. [Online]. Available: https://www.sciencedirect.com/science/article/pii/S0021979714003397

[73] Y. Hernandez, M. Lotya, D. Rickard, S. D. Bergin, and J. N. Coleman, "Measurement of Multicomponent Solubility Parameters for Graphene Facilitates Solvent Discovery," *Langmuir*, vol. 26, no. 5, pp. 3208–3213, Mar. 2010. [Online]. Available: https://doi.org/10.1021/la903188a

[74] L. Guardia, J. I. Paredes, S. Villar-Rodil, J. N. Rouzaud, A. Martínez-Alonso, and J. M. D. Tascón, "Discovery of effective solvents for platelet-type graphite nanofibers," *Carbon*, vol. 53, pp. 222–230, Mar. 2013. [Online]. Available: https://www.sciencedirect.com/science/article/pii/S0008622312008652

[75] L. Dai-Yang, M. Pengou, H. L. Tcheumi, D. Nguihdama, A. Wahabou, B. N. Ngatchou, O. R. T. Wamba, H. T. Kouamo, C. P. Nanseu-Njiki, and E. Ngameni, "Physico-Chemical and Electrochemical Characterizations of a Trachyte in the Far North Region of Cameroon for Possible Electroanalytical and Environmental Purposes," *Journal of Inorganic and Organometallic Polymers and Materials*, vol. 31, no. 2, pp. 542–551, Feb. 2021. [Online]. Available: https://doi.org/10.1007/s10904-020-01706-3

[76] S. Gunasekaran, G. Anbalagan, and S. Pandi, "Raman and infrared spectra of carbonates of calcite structure," *Journal of Raman Spectroscopy*, vol. 37, no. 9, pp. 892–899, 2006. [Online]. Available: https://onlinelibrary.wiley.com/doi/abs/10.1002/jrs.1518

[77] R. R. Nair, H. A. Wu, P. N. Jayaram, I. V. Grigorieva, and A. K. Geim, "Unimpeded Permeation of Water Through Helium-Leak–Tight Graphene-Based

Membranes," *Science*, vol. 335, no. 6067, pp. 442–444, Jan. 2012. [Online]. Available: https://www.science.org/doi/10.1126/science.1211694

[78] Y. Su, V. G. Kravets, S. L. Wong, J. Waters, A. K. Geim, and R. R. Nair, "Impermeable barrier films and protective coatings based on reduced graphene oxide," *Nature Communications*, vol. 5, no. 1, p. 4843, Sep. 2014. [Online]. Available: https://www.nature.com/articles/ncomms5843

Appendix A1

Supplementary data

A1.1 Zeta-potential distributions

Below, in Figure A1.1, are represented the ζ-potential distributions obtained for the six GO-init dispersions and the subsequent six GO-OL fractions refined from them. Measurements were made on prepared dispersions of the same concentration (0.25 mg/mL), in their respective solvents consisting of the water and ethanol mixtures. Noticeable differences can be observed between results obtained from dispersions in binary solvents, with a relatively large distribution, when compared to results from GO dispersions in water or ethanol.

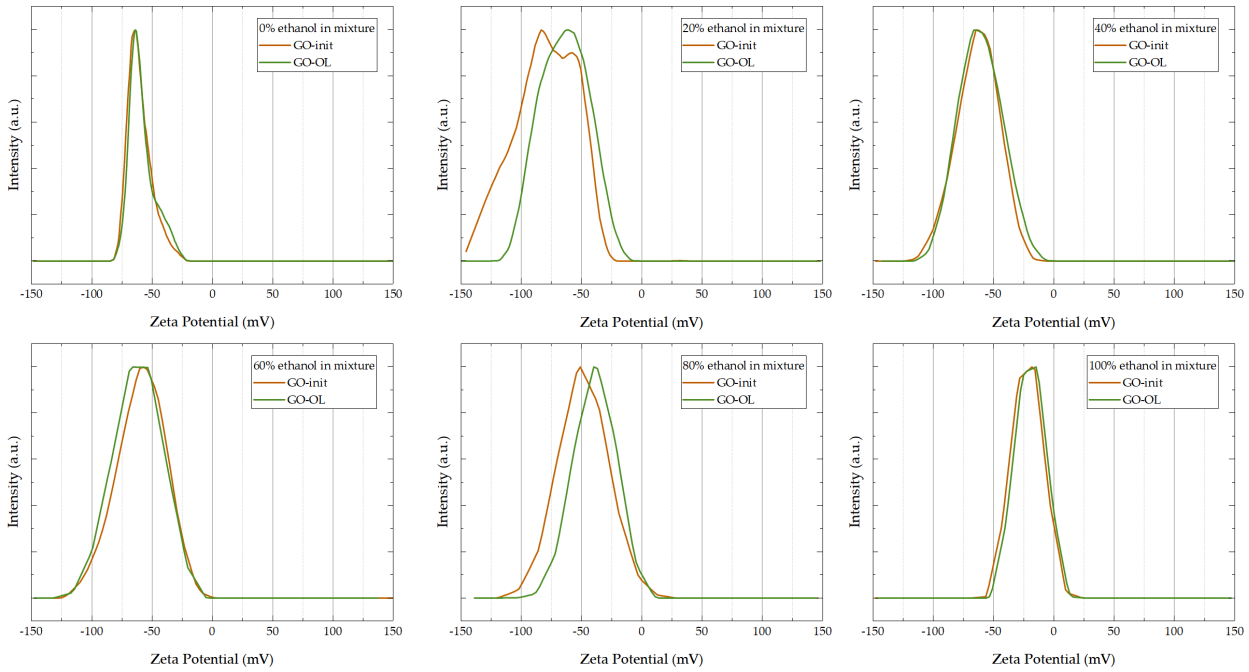

Figure A1.1: *ζ-potential distributions of the GO-init and GO-OL dispersions in their respective water/ethanol mixtures.*

A1.2 SEM images of GO self-assembled films

Figure A1.2 presents the morphology of the self-assembled GO-init and GO-OL films obtained from the 0%-40% ethanol dispersions. Similarly, Figure A1.3 presents the morphology of the self-assembled GO-init and GO-OL films obtained from the 60%-100% ethanol dispersions.

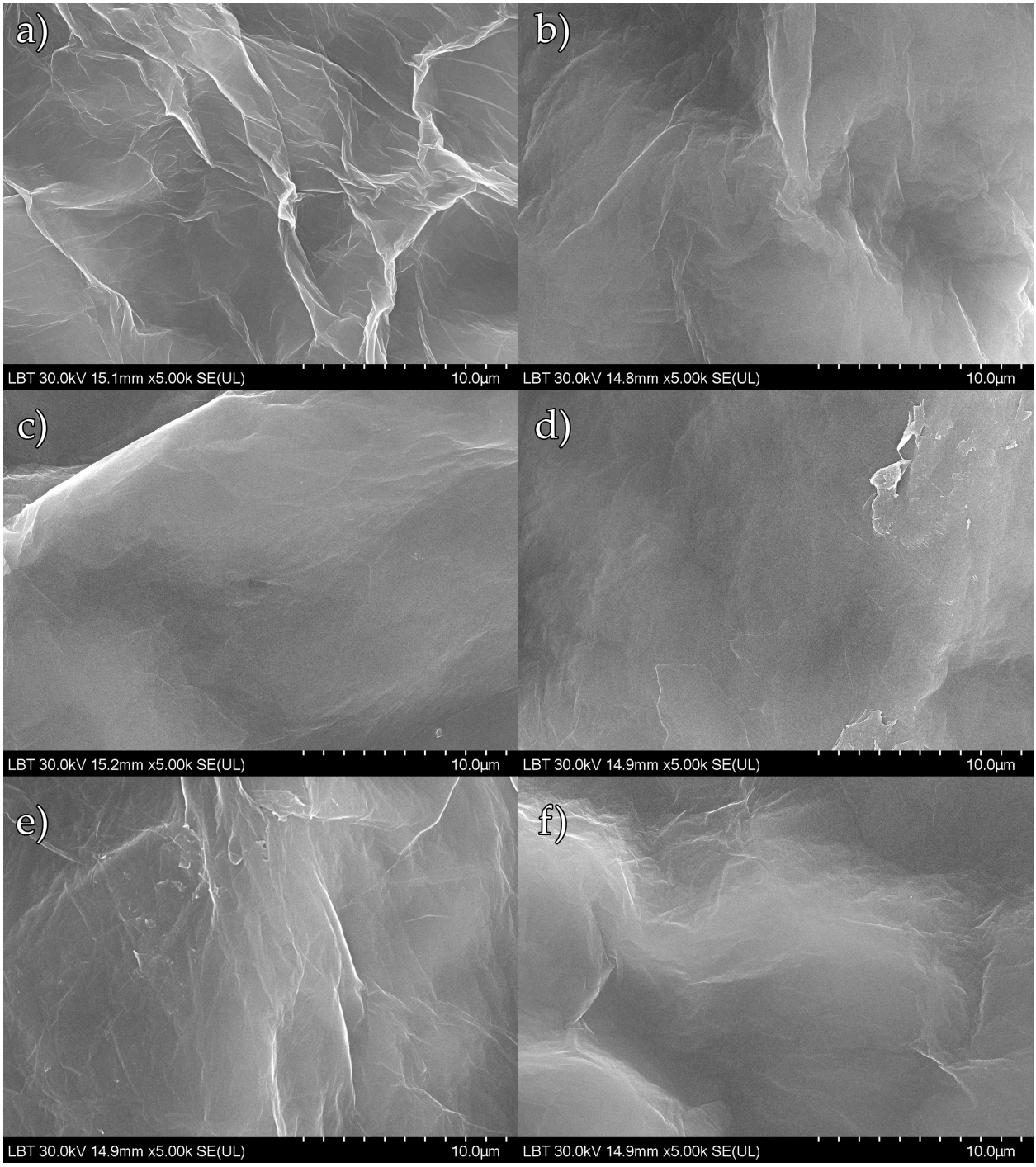

Figure A1.2: *SEM images of the morphology of GO-init (left side) and GO-OL (right side) self-assembled films films obtained from: a-b) 0% ethanol, c-d) 20% ethanol, and e-f) 40% ethanol dispersions.*

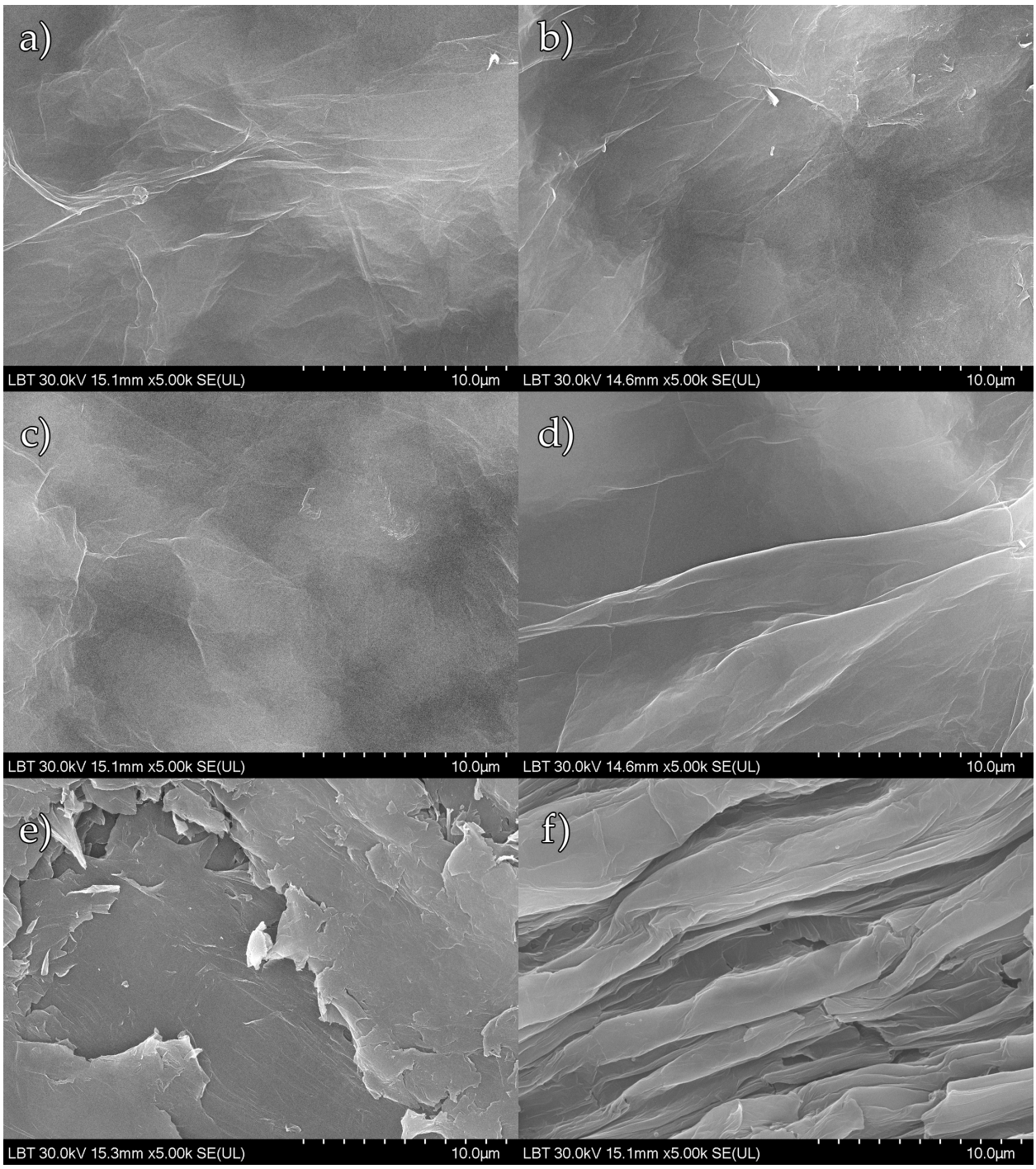

Figure A1.3: *SEM images of the morphology of GO-init (left side) and GO-OL (right side) self-assembled films films obtained from: a-b) 60% ethanol, c-d) 80% ethanol, and e-f) 100% ethanol dispersions.*

A1.3 Raman spectra

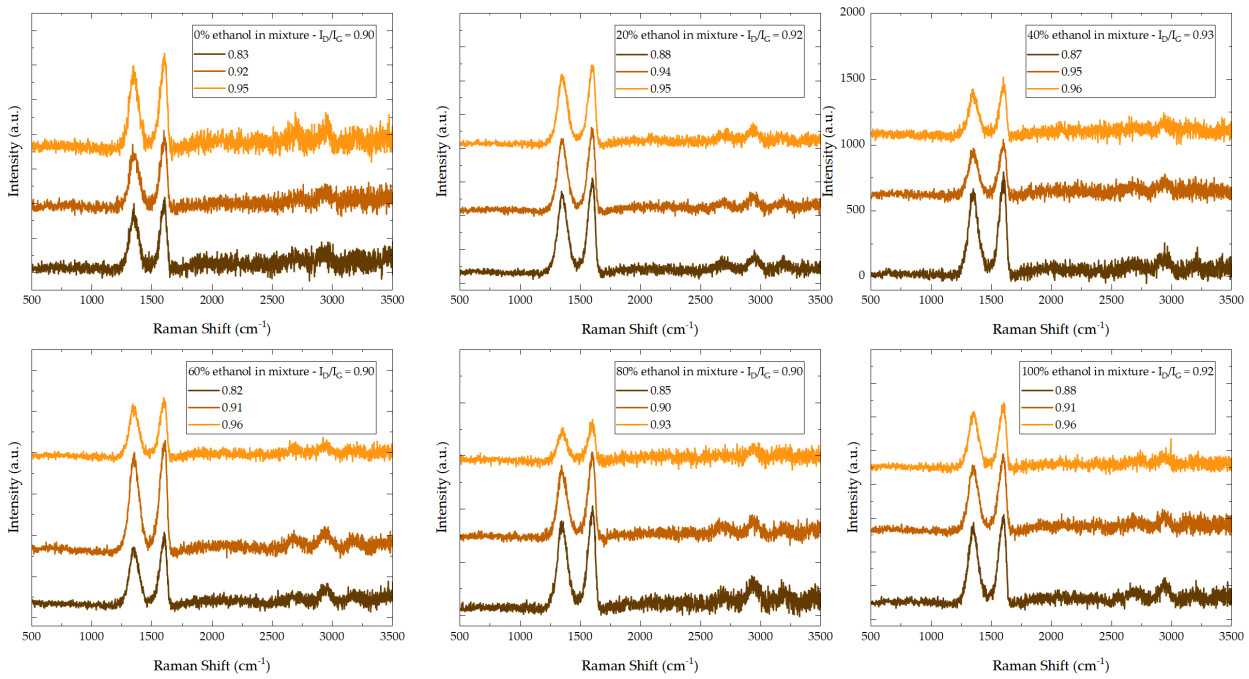

Figure A1.4: *Raman spectra obtained for the GO-init samples, with calculated I_D/I_G ratios.*

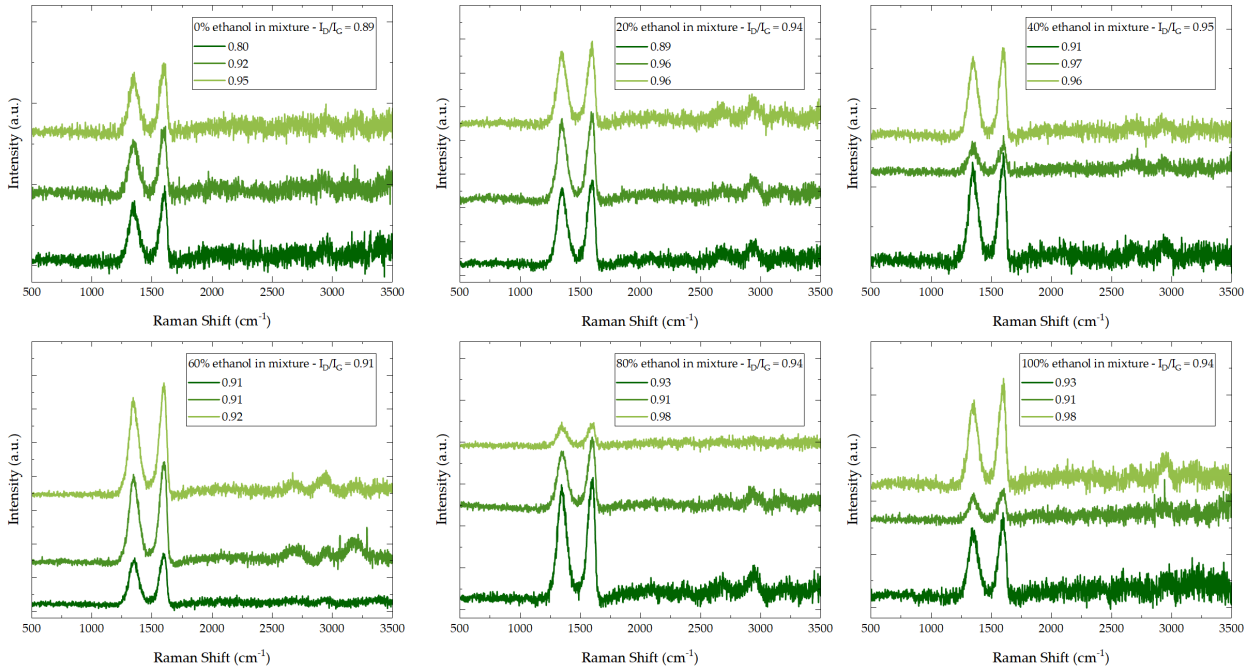

Figure A1.5: *Raman spectra obtained for the GO-OL samples, with calculated I_D/I_G ratios.*